Enabling Multi-Cation Electrolyte Usage in LMBs for Lower Cost and Operating Temperature

by

Allan Blanchard

Submitted to the Department of Materials Science and Engineering in partial fulfillment of the requirements for the

degree of

Bachelors of Science

at the

MASSACHUSETTS INSTITUTE OF TECHNOLOGY

June 2013

Signature of Author_____

Department of Material Science and Engineering
May 3, 2013

Certified by_____

Donald R. Sadoway
John F. Elliott Professor of Materials Chemistry
Thesis Supervisor

Accepted by_____

Jeffrey C. Grossman
Carl Richard Soderberg Associate Professor of Power Engineering
Chairman, Undergraduate Thesis Committee

Enabling Multi-Cation Electrolyte Usage in LMBs
for Lower Cost and Operating Temperature

by

Allan Blanchard

Submitted to the Department of Materials Science and Engineering
on May, 2013, in partial fulfillment of the
requirements for the degree of
Bachelors of Science

Abstract:

Alloy anodes form a promising path to the use of multi-cation electrolytes by increasing chemical stability. In this study, a lithium-magnesium alloy anode was developed such that lower cost and lower melting temperature multi-cation electrolytes could be incorporated in liquid metal batteries (LMBs). In a first part of this work, Lithium-magnesium was proven to be a viable anode in a standard uni-cation (Li^+) Li-Mg/LiCl-LiF-LiI/Sb-Pb battery. SEM and EDS confirmed the stability of this anode with respect to the cathode (Sb-Pb) and the standard uni-cation electrolyte. Performance metrics (voltage, efficiencies, etc.) for the Li-Mg anode cell were found to be comparable to the analogous pure Li anode system. In a second part of this work, using the alloyed Li-Mg anode, we demonstrated successful cycling of cells using multi cation electrolytes in Li-Mg/LiBr-KBr/Sb-Pb and Li-Mg/LiCl-KCl/Sb-Pb LMBs. Each of these multi-cation electrolyte systems boasted an active materials energy cost of (<150$/kWh), which is less expensive than the metric cost to implement storage batteries in the electrical grid.[1] These results open the door to incorporating lower cost and lower melting temperature electrolyte candidates in LMBs by using alloyed anodes.

Thesis supervisors: Donald R. Sadoway, Brice H. V. Chung

Titles: John F. Elliott Professor of Materials Chemistry, Research Scientist - TOTAL New Energies / visiting scientist at MIT

Acknowledgements

Firstly, I would like to thank my advisor, Professor Donald R. Sadoway, who has graciously allowed me to perform novel research in his group for the past two years. His continued mentorship and support has inspired me to learn the minute intricacies of the liquid metal battery technology and pursue the work in this study.

Secondly, I would like to thank my research supervisor Dr. Brice Chung. Interactions with Dr. Chung during this thesis endeavor have caused me to expand my creativity when tackling research problems and has pushed me to the limits of what I thought could ever be achieved with my skill set. I could not have accomplished this work without his mentorship and support.

In addition, prior to pursuing this thesis work, I had the pleasure of working very closely with Dr. David Bradwell, Dr. Takanari Ouchi, and Dr. Ulrich Muecke, the three of whom have provided me with a core skill set consisting of battery preparation, operation, and analysis. I am incredibly grateful for the experiences that I shared with these individuals because they helped to make me precise, relentless, but moreover, passionate, in regards to my research. The result of this had made my thesis work that much more rewarding.

I would also like to thank Prof. Kai Jiang, Dr. Kangli Jiang, Dr. Dane Boysen, Dr. Paul Burke, Dr. Gregory Thompson, Dr. Hojong Kim, Dr. Guillaume Lambotte, Dr. Satyajit Phadke, Dr. Douglas Kelley, Dr. Huayi Yin, Mr. Salvador Barriga, Ms. Jocelyn Newhouse, Mr. Brian L. Spatocco, and Mr. John Rogosic for giving me bountiful advice in electrochemistry and any research endeavor I partook in the group when needed. In addition, I would like to thank these graduate students, post doctorates, and professors for continually making the research environment within GroupSadoway warm, welcoming, and fun. I would also like to

acknowledge Mr. Jesus Moreno who was very helpful in preparing cell components used in various parts of this study. I am very grateful for his help.

Moreover, I would like to thank the multitude of friends I've encountered at MIT, especially those friends I've lived with at Alpha Delta Phi, who have supported me through my undergraduate journey at MIT and helped make my time here truly memorable.

Lastly, I would like to thank my parents, David and Florette Blanchard, who have seen me through it all and have been behind me 100% of the way. I could not have accomplished this feat without their love, support, and sacrifice. Along the same lines, I'd like to thank my brother David Jr., my sister Ashley, and the rest of my family for their continued love and support throughout my life.

TABLE OF CONTENTS:

LIST OF FIGURES

CHAPTER 4:

CHAPTER 5:

LIST OF TABLES

Chapter 1 – Introduction

Liquid metal batteries (LMBs) are a unique energy storage device currently being developed in group Sadoway as a means of improving the electric grid's reliability as well as supporting intermittent alternative energy sources (such as wind and solar). Due to their low cost, long lifespan, and rapid charge-discharge capability, LMBs are a particularly promising technology for remodeling our energy infrastructure. In addition, LMBs are novel in that they utilize three liquid layers: the cathode, anode, and electrolyte. These three layers can self-segregate by mutual immiscibility which provides a simple construction and hence potential ease of manufacturing. (Fig. 1.1)

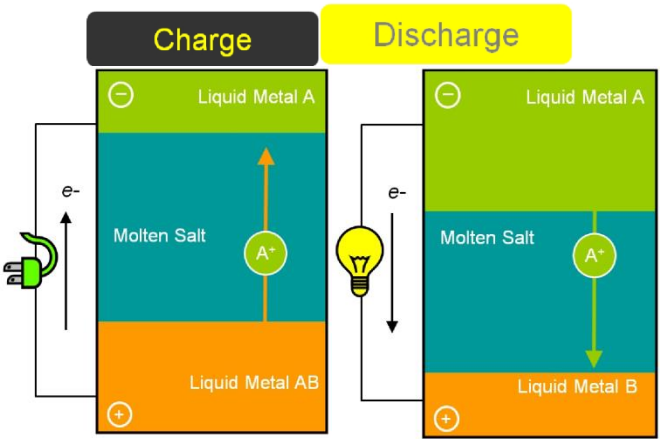

Figure 1.1: Diagram of a LMB in the charge and discharge state composed of three liquid layers: anode, electrolyte, and cathode shown from top to bottom respectively.

Important properties that the cell constituents must possess are that the electrode/electrolyte components should have relatively low melting points and be low cost. The container/insulation for the cell components must be chemically stable with the electrodes/electrolyte material and be able to withstand high temperatures (i.e. over 500^0C). [2] In

addition, it is prudent to select anode and cathode metals that maximize the cell voltage. Shown in Eq. 1.1, which follows from the Nernst Equation, a large cell voltage corresponds to a large activity difference between the anode and cathode material. For Eq. 1.1 ('V_{OCV}' is the open circuit voltage, 'R' is the ideal gas constant, 8.314J/mol-K, 'F' is Faraday's constant, 96,485 C/mol, '$a_{\underline{A}B}$' is the activity of the cathode composed of metal A dissolved in metal B (Fig. 1.1), and 'a_A' is the activity of the anode).

$$V_{\text{OCV}} = \Delta E = \frac{RT}{nF} \ln\left(\frac{a_{\underline{A}B}}{a_A}\right) \qquad \text{(Eq. 1.1)}$$

Thus, possible candidates for cathode and anode materials are conveyed in Figure 1.2 and are based off of optimizing the difference in activity discussed. This thesis will focus on a promising chemistry (Li/electrolyte/Sb-Pb), capable of meeting the low target active materials cost of 150$/kWh, energy efficiency of over 70%, and a stringent low target fade rate (<0.02%/cycle) necessary for implementation in the energy grid.[1]

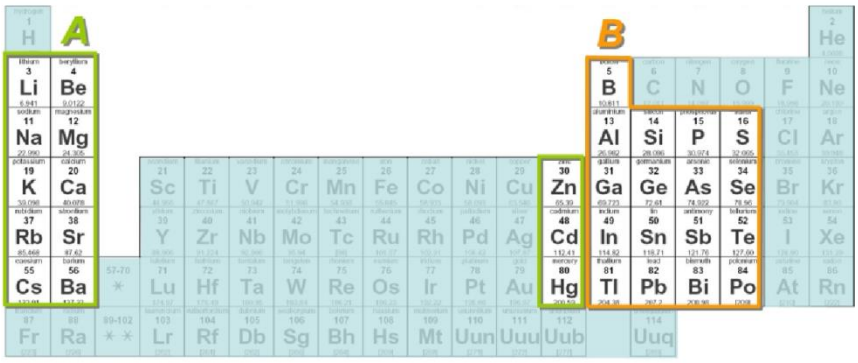

Figure 1.2: Diagram depicts possible candidates for metal A (Figure 1 anode material) and metal B (Figure 1 cathode material) from the periodic table.

1.1 Opportunity for Lower Cost and Lower Temperature LMBs

Currently, there is an opportunity to significantly reduce the cost and operating temperature of LMBs even further. Previous work done has shown that the electrolyte component of standard cells (Li/electrolyte/Sb-Pb) possess the highest melting temperature of the active materials, represents a major portion of the cell cost, and can largely affect the performance of the cell. Thus, choosing the right electrolyte material is key to optimizing the operating temperature, cost, and performance of standard cell LMBs.

The major challenge in incorporating alternative electrolyte candidates is the high reactivity of pure lithium. Shown in Table 1.1, there exists a large selection of suitable candidate electrolyte that are lower melting ($<450^0$C) and lower cost (<50$/kWh). [2] Some of the most attractive candidates highlighted in Table 1.1 exhibit costs (~30$/kWh) and melting temperatures of 350^0C. These electrolytes are multi-cation electrolytes, a mixture of salts that include the itinerant specie (Li^+) but also other cation salts (e.g. K^+, $Na^{+,}$ etc.). These multi-cation electrolytes can tremendously help lower the cost and melting temperature of LMBs.

Table 1.1: Molten Salt Electrolyte Cost Trajectory and Melting Temperature Data

Candidate Electrolyte	Composition (mol%)	[α] Melting Temperature (^{0}C)	[β] Estimated Density [T> Tm] (g/cm^3)	[γ] Estimated Cost ($/kWh)
LiCl-KCl	59-41	350	1.51	29.22
LiF-LiCl-KCl	2-59-39	350	1.52	30.02
LiBr-KBr	60-40	325	2.37	31.52
LiCl-KCl	67-33	425	1.51	32.54
LiF-LiCl-KBr	2-60-38	350	1.75	35.62
LiCl-LiF-LiBr	31-22-47	430	2.05	41.09
LiCl-LiF-LiBr	45-25-30	450	1.89	44.50
LiF-LiCl-NaCl	23-66-11	495	1.58	44.72
LiF-LiCl-NaF	12-77-11	490	1.59	48.12
LiCl-LiF	45-55	500	1.67	56.17
LiCl-LiF-LiI	68-24-8	490	1.70	1197.85
LiCl-LiF-LiI	50-20-30	400	2.05	3599.12

[α] Melting temperature data was retrieved from Masset et al.[3] [β] Density data was estimated using data from Janz G. J.[4] [γ] Cost data was estimated assuming same battery performance for all chemistries, volume of electrolyte, and cost derived from bulk quotations from suppliers (outlined further in section 6).

In the case of LiCl-KCl multi-cation electrolytes it is well documented that the displacement reaction, shown in equation 1.2, between metallic lithium and potassium chloride molten salt is prone to occur in high temperature (~450^{0}C) batteries.[3] Similar reactions between lithium and halides containing (K or Na) cations account for why many multi-cation salts, shown in Table 1.1, are unstable with lithium anodes in high temperature batteries. Conversely, all of the Li^+ uni-cation electrolytes shown in Table 1.1 were successfully demonstrated in (Li/electrolyte/Sb-Pb) LMBs. Thus, developing a way in which multi-cation salts can be incorporated in LMBs provides a means of reducing the operating temperature and cost of these batteries. This is the goal at the heart of my thesis.

$$Li^0_{(l)} + K^+ + Cl^- \rightarrow K^0_{(g)} + Li^+ + Cl^- \qquad \text{(Eq. 1.2)}$$

1.2 Experimental Approach

The switching mechanism between lithium and other metal cations in the electrolyte largely determines the stability of the anode with respect to a multi-cation electrolyte. This switching mechanism, shown in Eq. 1.3 for a generic electrolyte composed of LiX-MX, is controlled by the reactivity of lithium in the anode and the operating temperature. The higher the effective reactivity is of lithium in the anode and the higher the operating temperature is, the more favorable it is for the lithium displacement reaction to occur. Thus, the experimental approach was first to develop an anode of lithium alloyed with another candidate metal in effort to reduce the activity of the anode and the effective reactivity of pure lithium. Secondly, once a suitable alloy anode was developed and demonstrated with a uni-cation electrolyte, lower melting temperature multi-cation electrolyte candidates were considered in effort to reduce the total operation temperature of the cell. The combination of reducing the activity of the anode and the operation temperature of the cell in this stepwise manner would best serve to limit lithium displacement reactions that occur when using multi-cation electrolytes. In addition, explicated in "Liquid Metal Batteries: Past, Present, and Future", thermodynamically this approach also helps limit the solubility of lithium in multi-cation electrolytes.[5]

$$Li^0{}_{(l)} + M^+ + X^- \rightarrow M^0{}_{(g)} + Li^+ + X^- \qquad \text{(Eq. 1.3)}$$

Considerations when using an alloy anode in LMBs are that one must expect the activity of the alloy anode to be lower than the activity of pure lithium such that, following from Eq. 1.1, an associated cell voltage penalty will result when compared to the pure lithium anode system. In addition, cost of the candidate metals for the anode and the candidate multi-cation electrolytes

must be considered such that the batteries that result from this study are valuable for industrial applications.

1.3 Experimental Setup

A diagram of the 1Ah scaled batteries used for testing in this thesis is shown in Figure 1.3. All the base components were initially cleaned by sonicating in acetone and manual wiping with aid of acetone and kimwipe. The active materials of the battery were added inside a glovebox filled with argon, (O_2 levels < 2ppm, and H_2O levels < 0.5 ppm). The glovebox had an attached furnace where cells were placed when fully assembled and ready for operation shown in Figure 1.4 (A). A maximum of four cells could fit in a single furnace at one time so each of the tests outlined in this study reflect a batch of four cells which operated simultaneously. Each cell was labeled with YearMonthDate-Operator's Initials-Cell Number shown in Figure 1.4 (B) using a scribe pen.

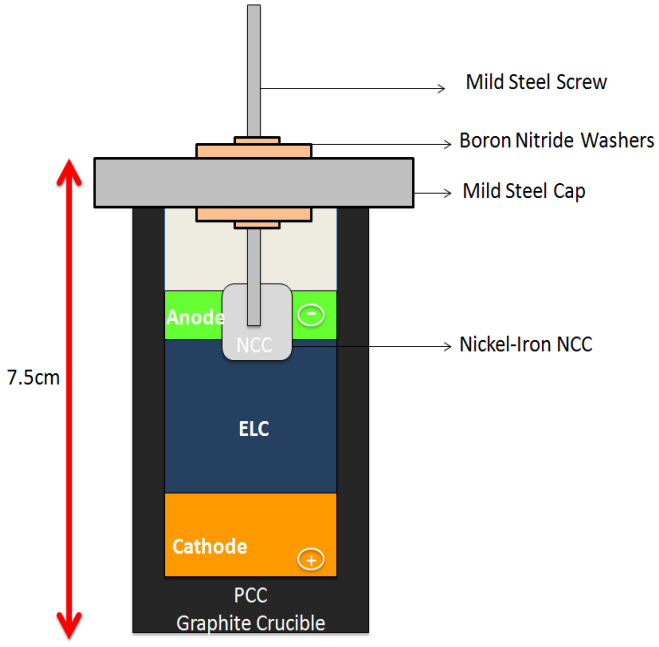

Figure 1.3: Diagram depicts the components of 1Ah scaled battery and gives an approximate height from end of the cap to the end of the graphite crucible. PCC stands for positive current collector and NCC stands for negative current collector in this diagram.

(A) (B)

Figure 1.4: (A) Picture of glovebox and attached furnace used for testing. (B) Picture of a batch of four cells labeled after base component cleaning. It is important to note that these four cells, with mild steel PCC, were not used for this study and are simply to demonstrate labeling procedure.

For processes that involved forming Sb-Pb or anode alloys, use of an induction furnace, shown in Figure 1.5 contained within an argon filled glovebox, was essential. This induction furnace proved to reach temperatures well over 650^0C. Moreover, cells were connected with four leads, two positive and two negative, to an Arbin Instruments machine which regulated cell cycling and periodically recorded data. There were two methods of connecting leads to each cell (1) involved screw clamps that had the two positive leads touching each other as well as the two negative leads and (2) involved four set screws that had each lead individually connected to the cell. The first method which involves the leads touching adds an extra resistance factor due to the

fact that there is resistance between the wires one needs to consider. This method was only used for one test in this study in effort to avoid this phenomenon.

For post mortem analysis cells were cooled down and cut with a ceramic blade saw shown in Figure 1.6. After being cut, pictures were taken of the cells to analyze mechanisms of failure. Then the cells were quickly dipped in isopropanol, wiped to remove surface impurities (carbon, saw bits, oil, mild steel), and finally placed under vacuum in preparation for Scanning Electron Microscopy (SEM) and Electron Dispersive Spectroscopy (EDS). Since the saw blade used to cut the cells was not swapped out for each batch of cells and the isopropanol partially dissolves some of the electrolyte it is expected that there be some slight impurities or irregularities indentified in EDS reports. Nevertheless, a (JEOL 6610LV) SEM/EDS machine was used to quantify the active material composition. It is important to note that EDS is unable to identify lithium and is only accurate within ~1-2 atomic% in regards to compositional analysis.

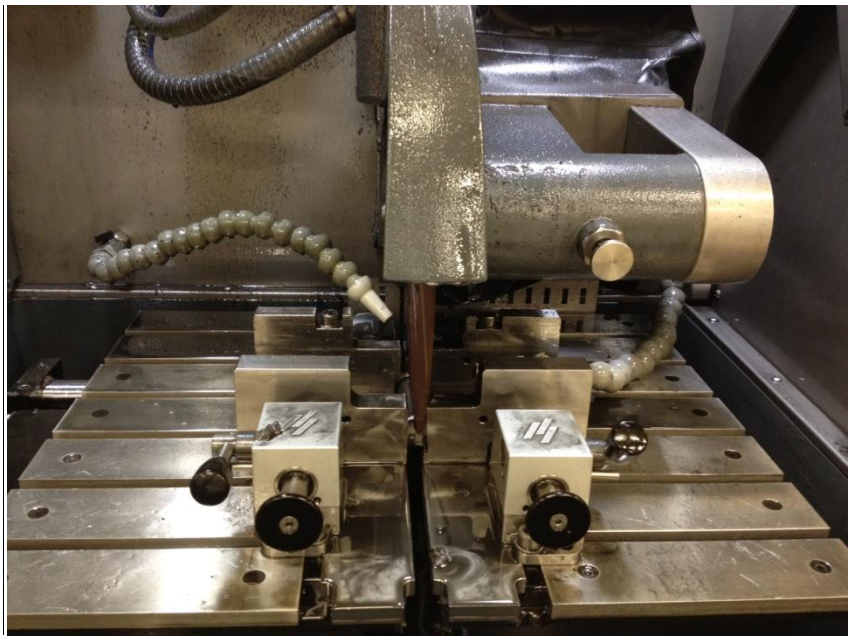

Figure 1.5: Picture depicts ceramic blade saw used to cut cells post-mortem.

Chapter 2 – Alloy Anode Functionality

Conveyed in section 1.2, using an alloy anode of lithium with another candidate metal could provide a means of limiting the reactivity, and solubility of lithium in the presence of multi-cation electrolytes. Proof of concept of the use of an alloy anode and a multi-cation electrolyte in high temperature batteries was already demonstrated in a Li-Al/FeS cell with a LiCl-KCl electrolyte at about 450^0C. [6]

2.1 Determining Alloy Composition

Criteria for selecting candidate lithium alloy anodes were that they needed to be able to provide a large window over which lithium could discharge out of the anode while remaining in the liquid phase around 450^0C or below. In addition, it was important that alloy anode candidates formed stably and were inert with the different secondary non active components of the cell such as the current collector, the graphite crucible, and the boron nitride washers. Moreover, stated in section 1.2, there exists an open circuit voltage penalty associated with decreasing the activity of an anode. Thus, it was important that alloy anode candidates provided an optimal balance in reducing the activity of the anode to decrease anode reactivity with electrolyte, while maintaining a high enough activity such that there is minimal voltage penalty for the battery.

Mg, Al, Si, Sn, Sb were all considered good metal candidates to alloy with lithium in that they are cost-effective, abundant, and environmentally friendly.[7] Figure 2.1 conveys the approximate potential difference between a pure lithium electrode and the candidate electrodes stated above. From data depicted in Figure 2.1 and use of Equation 1.1 (Nernst Equation) it is clear that magnesium possesses an activity that is, although lower than that of pure lithium, very

close in value to that of pure lithium. Thus, magnesium would provide the lowest voltage penalty out of all the candidates.

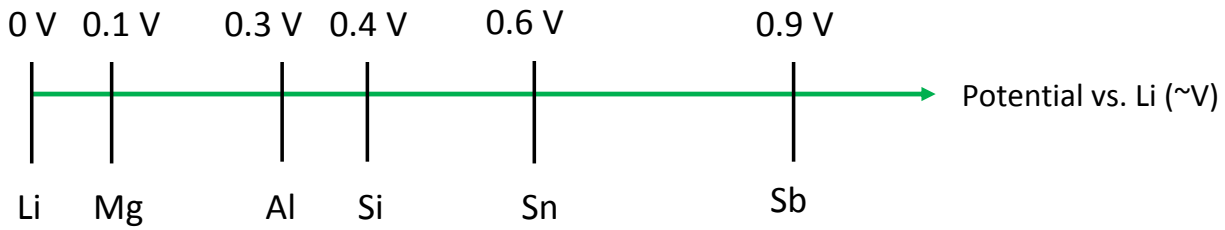

Figure 2.1: Depicts the potential of several candidate metals in reference to lithium. Data retrieved from work done by Zhang W.-J.[7]

In addition, at standard operation temperature (~450^{0}C), Li-Mg alloys possess a wide compositional range in the liquid phase. (Figure 2.2) Aluminum was still considered as a viable candidate and had a strong appeal in that a Li-Al anode has been demonstrated to work with a multi-cation electrolyte in a Li-Al/FeS cell at 450^{0}C.[6] However, a Li-Mg alloy was ultimately selected as the optimal anode because it provided an opportunity to create cells with minimal voltage penalties. Also, very little literature was found regarding the use of Li-Mg alloys in high temperature batteries so there was an added incentive to bring new-found knowledge to this community of research.

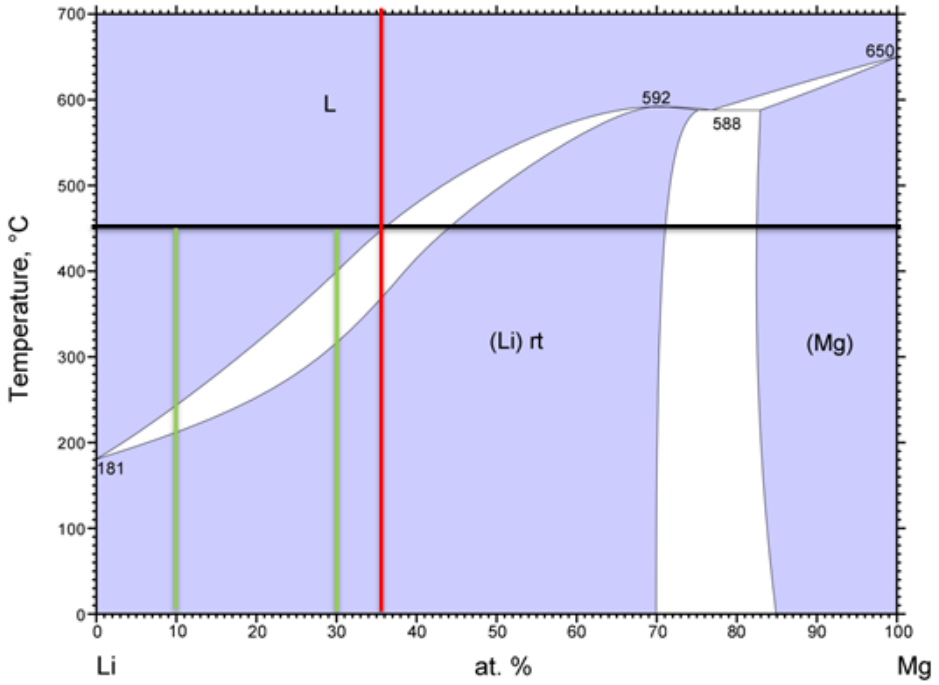

Figure2.2: In this diagram the green lines depict the region over which the lithium magnesium anode was designed to discharge such that anode could safely remain in the liquid state at 450^0C. The red line marks the composition boundary at which the alloy anode starts to become solid at 450^0C.[8]

The Li-Mg anode composition that was chosen for experimental purposes is shown in Figure 2.2. The anode was designed to discharge from 90-10 mol% lithium at 450^0C such that a considerable amount of lithium could discharge and give the battery sufficient capacity while remaining in the liquid state. The lithium concentration in the charged state was limited to 90 mol% to avoid achieving an anode activity close to that of pure lithium.

2.2 Testing Li-Mg Anode Functionality in LMBs

2.2.1 Forming Li-Mg Alloy Anode

To form the alloy anode, a mixture of lithium and magnesium in a 90-10 mol% ratio was heated in a glovebox to above 650^0C using an induction furnace. The alloy formed homogenously and no chemical instability was visually observed during the process.

2.2.2 Materials, Test Plan, and Expectations

The active components used for this test are shown in Figure 2.3. It was expected that the Li-Mg/LiCl-LiF-LiI/Sb-Pb system would demonstrate high chemical stability between its active components while achieving comparable efficiencies as its counterpart unalloyed anode Li/LiCl-LiF-LiI/Sb-Pb system. The Li/LiCl-LiF-LiI/Sb-Pb cell system was previously demonstrated to yield 98% coulombic and 67% voltage efficiencies at 450^0C and 0.280 A/cm^2.[4] SEM, EDS, and cycling performance were used to confirm battery functionality and active component stability.

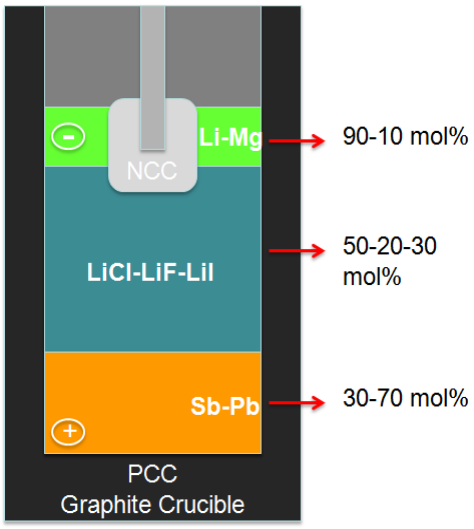

Figure 2.3: Describes compositions of the active materials within cells for the Li-Mg anode functionality test. All active materials were formed using high purity laboratory grade constituents (>99.9% pure).

2.2.3 Li-Mg Cycling Data

The Li-Mg/LiCl-LiF-LiI/Sb-Pb system achieved 120 charge/discharge cycles while maintaining a low and stable resistance profile. (Figure 2.4) This indicates that the electrodes were stable with the electrolyte and no extraneous interactions occurred. The resistance for this system (~0.1 Ohms) is higher than that for the Li/LiCl-LiF-LiI/Sb-Pb system (~0.03 Ohms); however, along with likely overpotentials associated with alloying/dealloying Li from the LiMg anode, it is important to note that the Li-Mg cells used screw clamps instead of set screws for the lead connection which most likely resulted in increased cell resistance, discussed further in section 1.3.

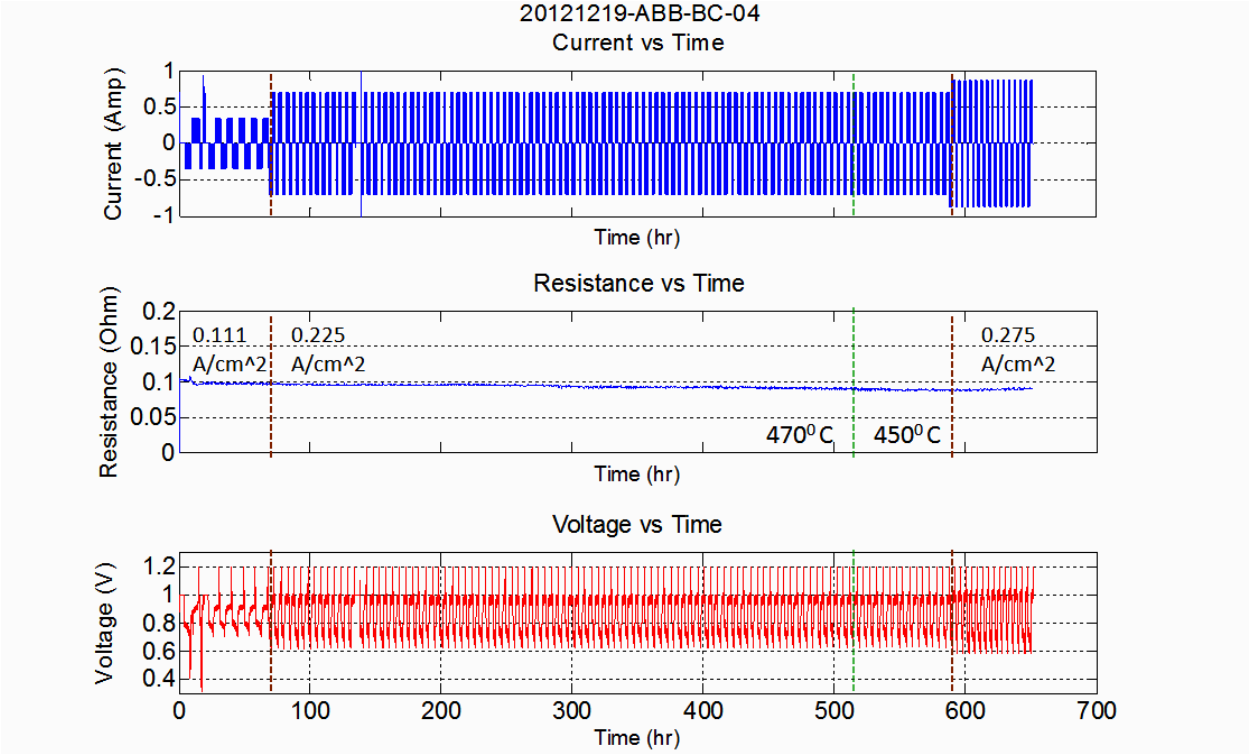

Figure 2.4: Depicts current, resistance, and voltage data for a Li-Mg/LiCl-LiF-LiI/Sb-Pb cell. Green dashed lines represent where temperature transitions occur and brown dashed lines represent current transitions.

Moreover, the Li-Mg/LiCl-LiF-LiI/Sb-Pb system was capable of maintaining an energy efficiency of 63% and columbic efficiency of 97% for a current density of 0.275 A/cm^{2}at 450^{0}C. (Figure 2.5 (A)) These results are in line with the 67% energy and 97% columbic efficiencies obtained with the unalloyed Li/LiCl-LiF-LiI/Sb-Pb system for the same conditions. [4] In addition, operating under the same conditions, the Li-Mg/LiCl-LiF-LiI/Sb-Pb cell consistently achieved 93% theoretical capacity when discharging and 96% theoretical capacity when charging per cycle. (Figure 2.5 (B))

(A) (B)

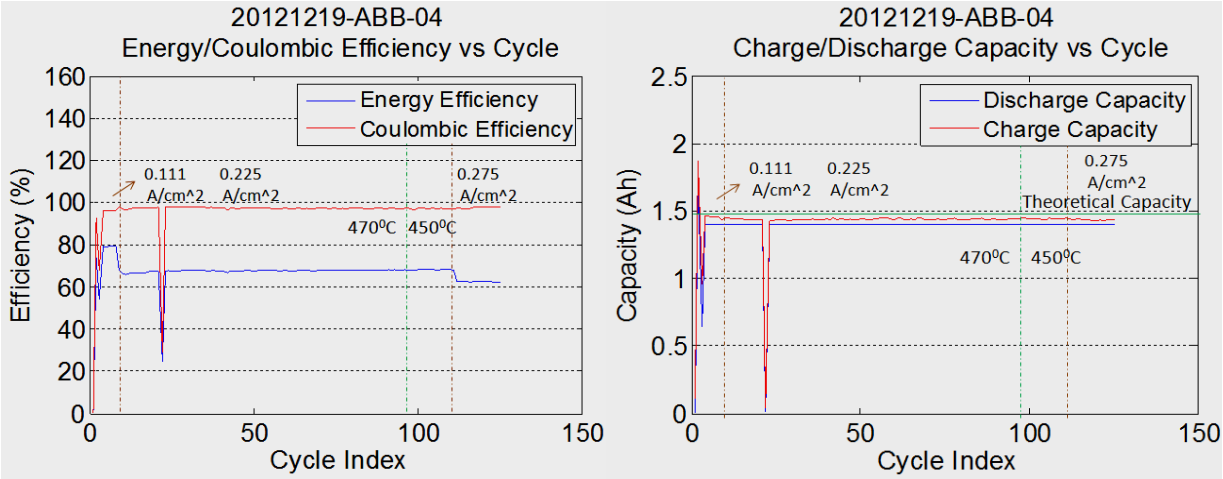

Figure 2.5: For both plots the green dashed lines mark temperature transitions while the brown dashed lines mark current transitions. (A) Depicts the energy and coulombic efficiency for the Li-Mg/LiCl-LiF-LiI/Sb-Pb system over a range of temperatures and currents. Drastic spikes in this plot correspond to leakage current measurements. (B) Depicts the capacity utilization for the Li-Mg/ LiCl-LiF-LiI/Sb-Pb system over a range of temperatures and currents. Theoretical capacity is labeled with a solid green line. Spikes in this plot that reach zero (Ah) correlate to moments where leakage current measurements were taken.

At 450^{0}C and 0.275 A/cm^2, the Li-Mg/LiCl-LiF-LiI/Sb-Pb charge voltage is (~0.03 V) larger than the standard cell, Li/LiCl-LiF-LiI/Sb-Pb, charge voltage and the discharge voltage is (~0.07 V) smaller than the standard cell discharge voltage. (Figure 2.6) This confirms that there is a small voltage penalty associated with using a Li-Mg anode versus a pure lithium anode,

which is what was expected. It is important to note that there may be additional diffusion and charge transfer potential penalties that can further account for the Li-Mg voltage profile observed in Figure 2.6.

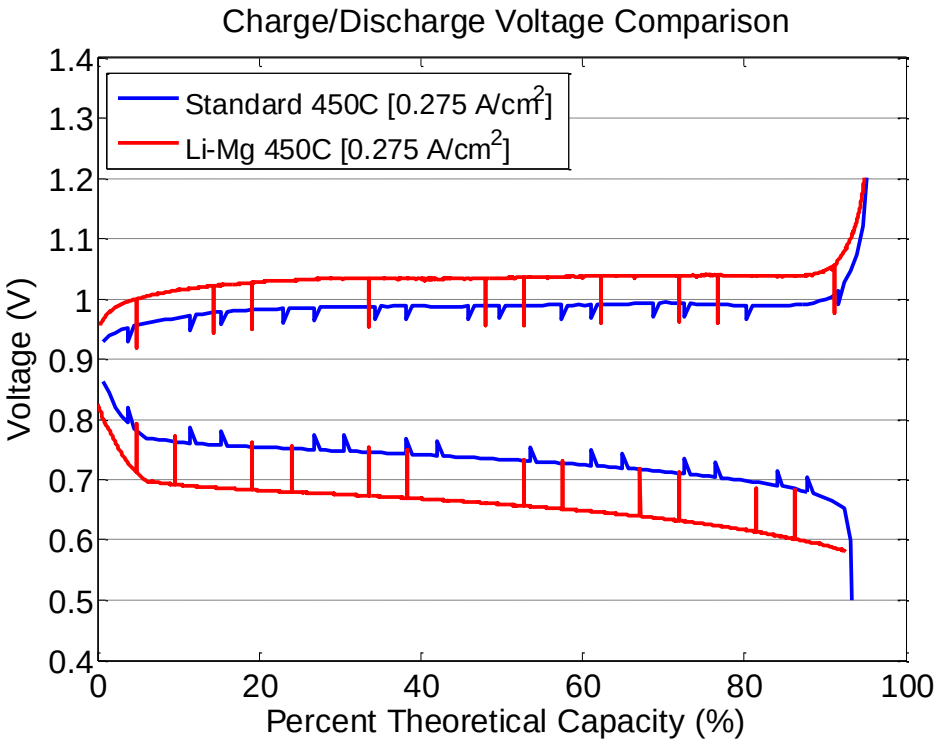

Figure 2.6: Depicts the cell voltage (V) versus percent theoretical capacity (%) for the Li/LiCl-LiF-LiI/Sb-Pb system labeled standard and the Li-Mg/LiCl-LiF-LiI/Sb-Pb system labeled Li-Mg Anode. The spikes in this plot correspond to instances where resistance measurements were taken.

2.2.4 Li-Mg Post-Mortem Analysis

Cell 20121219-ABB-04 was manually stopped while in the complete charge state shown in Figure 2.7. In addition, post-mortem, a large supply of electrolyte was found to still exist within the cell. (Figure 2.7) SEM and EDS were performed on cell 20121219-ABB-04 shown in Figure 2.8 and 2.9. The purpose of the EDS analysis was to see how well the post-mortem compositions in the cell corresponded with the designated compositions for the active components of the cell depicted in Figure 2.3.

Figure 2.7: Picture of a 20121219-ABB-04 cell post-mortem, scale is in units of centimeters. This cell was manually stopped while in the complete charged state.

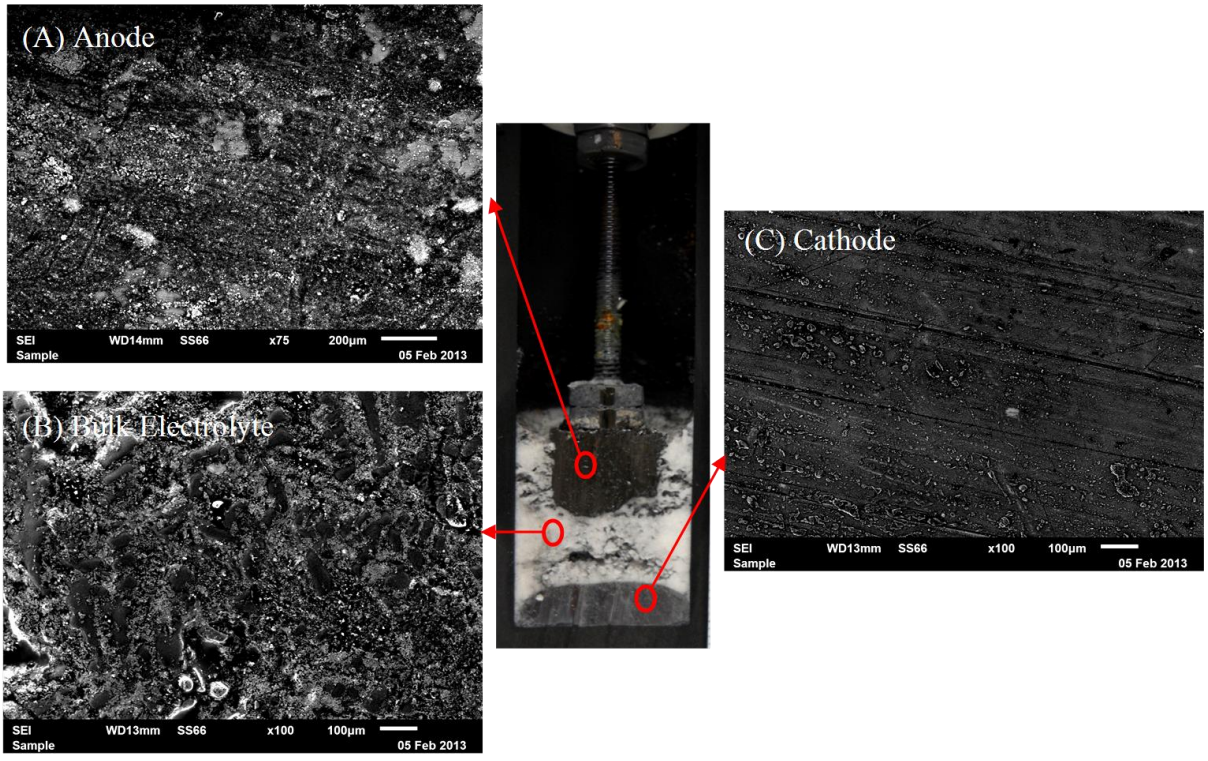

Figure 2.9: Depicts SEM images for (A) Anode, (B) Bulk Electrolyte, and (C) Cathode regions of the cell. A scale bar is located at the lower right edge of each picture. The corresponding values associated with the scale bars are (A) 200µm (B) 100µm and (C) 100µm.

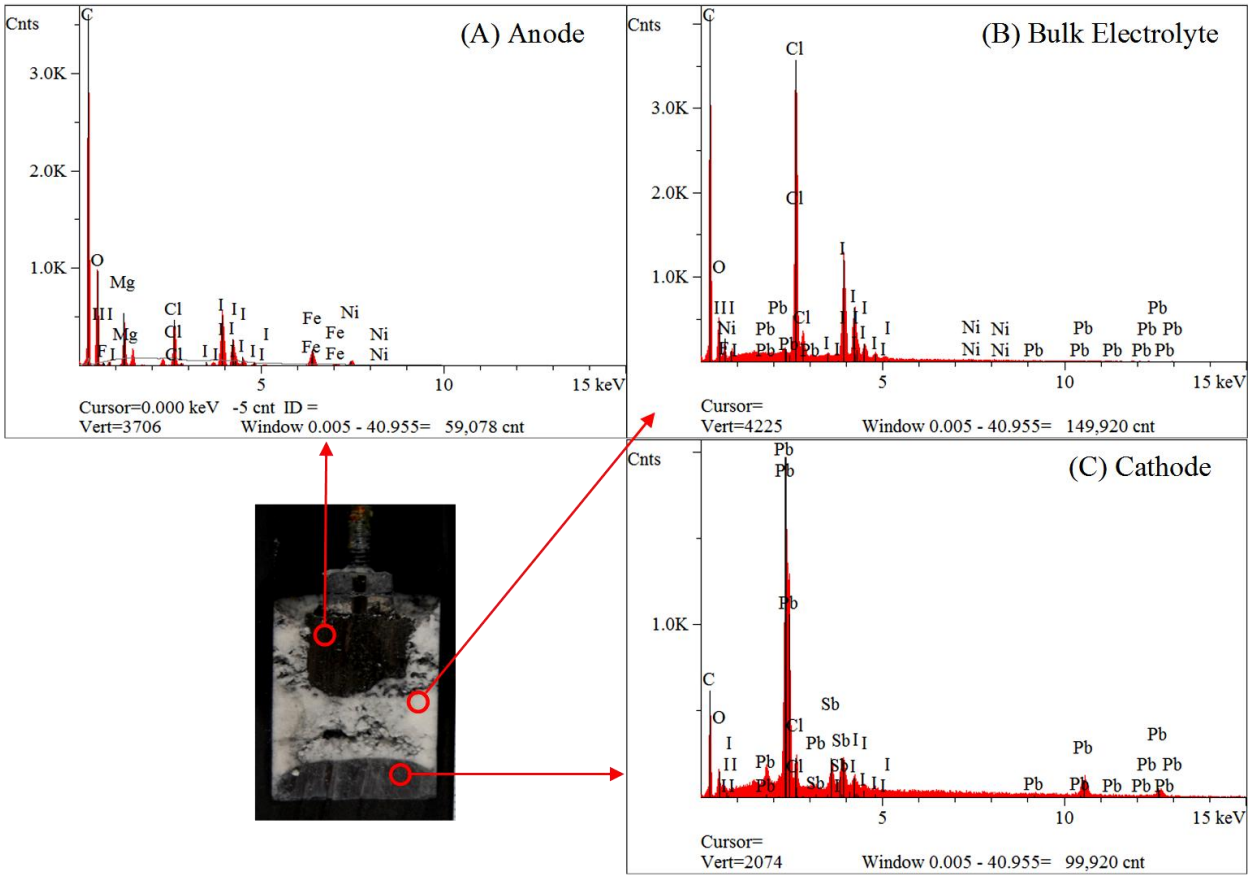

Figure 2.8: Depicts EDS plots output for (A)Anode, (B) Bulk Electrolyte, and (C) Cathode regions of the cell at 20.0 kV and a 35^0 takeoff angle. Plots correspond to SEM images in Figure 2.8. The elapsed livetime values associated with each plot is (A) 42.0 (B) 37.2 and (C) 12.8 seconds.

The designated anode composition, in the fully charged state, was 90-10 mol% lithium-magnesium. Due to EDS detection limits, lithium could not be detected; however; the post-mortem composition of the anode was found to be primarily magnesium, iron and nickel (which comprise the negative current collector), and what is most likely electrolyte contaminants present due to EDS sample preparation, explained further in section 1.3. (Table 2.1) Thus, the results in Table 2.1 match with what was expected to comprise the anode.

The designated electrolyte composition was 50-20-30 mol% LiCl-LiF-LiI. The post-mortem composition of the bulk electrolyte in atomic% was found to be 50.0% chlorine, 19.5% fluorine, and 27.3% Iodine. (Table 2.1) This corresponds well with the designated composition

of the electrolyte. In addition, the composition of the cathode was designed to be 30-70 mol% antimony-lead. At post-mortem stage, the ratio of antimony to lead was found to be 34-66 atomic%. This also corresponds well to the designed composition of the cathode. (Table 2.1) Other constituent elements that were detected in the cathode aside from antimony and lead are most likely due to electrolyte contamination due to EDS sample preparation.

Moreover, Figure 2.9 conveys how there are no observable peaks for magnesium in the bulk electrolyte or the cathode. In addition, the EDS data shown in Table 2.1 for the bulk electrolyte and cathode regions have values of (<1.5 atomic%) for magnesium, which indicates that the presence of magnesium in these regions are most likely negligible due to EDS detection limits. Since, post-mortem, there were negligible traces of magnesium in the bulk electrolyte and the cathode it indicates that magnesium is stable in the Li-Mg/LiCl-LiF-LiI/Sb-Pb cell.

Table 2.1: EDS Data for Anode, Bulk Electrolyte, and Cathode Regions

Elements	**Anode Composition (Atomic %)**	**Bulk ELC Composition (Atomic %)**	**Cathode Composition (Atomic%)**
Magnesium	35.0	0.9	1.3
Iron	11.3	-	-
Nickel	4.8	0.3	-
Chlorine	15.0	50.0	7.8
Fluorine	6.6	19.5	-
Iodine	27.3	28.8	18.7
Lead	-	0.5	53.8
Antimony	-	-	18.3
	100	100	100

2.3 **Li-Mg LMB Functionality Summary**

The Li-Mg/LiCl-LiF-LiI/Sb-Pb system achieved over 120 cycles demonstrating energy efficiencies of 63% and columbic efficiencies of 97% at 450^0C and 0.275 A/cm^2. These results are in line with the 67% energy and 97% columbic efficiencies achieved by the unalloyed anode Li/LiCl-LiF-LiI/Sb-Pb system for the same conditions.[4] In addition, the Li-Mg anode was confirmed through EDS and SEM to be stable with the electrolyte and cathode components of the cell (i.e., negligible traces of Mg were found in electrolyte and cathode) after cycling over 120 cycles. Lastly, the Li-Mg anode observed an expected small voltage penalty of (~0.03V) in the charged state and (~0.07V) in the discharge state. Thus, the Li-Mg is deemed a highly functional anode when paired with uni-cation electrolytes in LMBs.

Chapter 3 – Selecting Multi-Cation Salts to Test in LMBs

In selecting multi-cation salt candidates it was necessary to find candidates that were theoretically very stable in the presence of lithium and could provide an opportunity for a large cost reduction of the cell. Potassium was seen as a good candidate cation to have in a multi-cation salt because shown in Table 1.1 the multi-cation salts that contained potassium were the cheapest and the lowest melting electrolytes. For this study, the goal was to pair a candidate potassium halide with its counterpart lithium halide to form a multi-cation salt for testing.

3.1 Electrolyte Candidate Cost and Stability Comparison

The stability of a potassium halide in the presence of lithium is closely related to the Gibbs Free Energy of Formation of a specific KX halide versus its counterpart LiX halide. The difference in Gibbs Free Energy of Formation between several KX and LiX halides versus temperature is depicted in Figure 3.1. In Figure 3.1, the energy of formation values were converted to potential (V) on the y-axis through the equation,

$$\Delta G = -nFE \qquad \text{(Eq. 3.1)}$$

where ΔG is the Gibbs Free Energy Change, n is the number of moles, F is Faraday's constant 96,485 C/mol, and E is the potential. Thus, Figure 3.1 conveys how over a temperature range of 100^0C to 700^0C the KX halide candidates (KBr, KCl, KI) are theoretically stable in the presence of pure lithium because these halides are thermodynamically more favorable to form over their counterpart LiX halides. Additionally, according to this analysis, KF is more unfavorable than LiF over the same temperature range and should be avoided as a candidate electrolyte component. The stability ranking for the potassium halide candidates is, listed from left to right

in decreasing stability, KI, KBr, and KCl. It is important to note that there is a general trend with increasing temperature that the KX halides become more unfavorable to form, or less stable, with increasing temperature. (Figure 3.1) In addition, in regards to batteries, under polarization of the system, the KX halides may become less stable due to the potential associated with the $\Delta G_{KX} - \Delta G_{LiX}$. Additional considerations on alloying potentials and competing reactions need to be made to draw a full conclusion and is beyond the scope of this thesis.

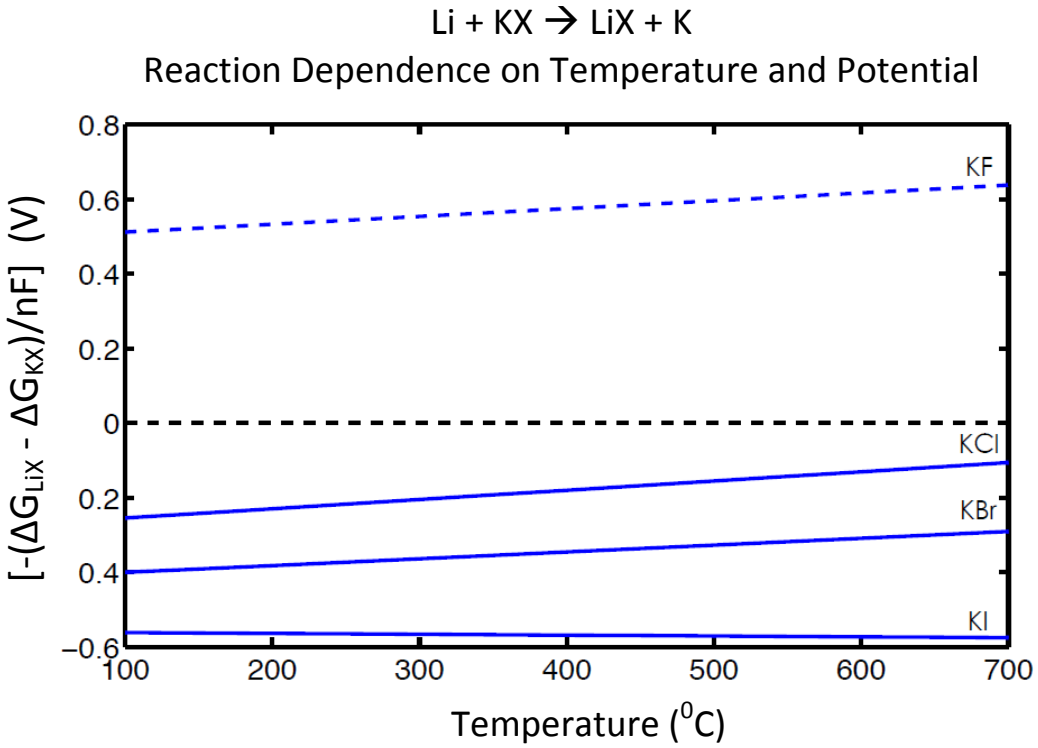

Figure3.1: The distance from the blue line to the black dashed line depicts the voltage above which the lithium counterpart of the potassium halides labeled is more favorable. As temperature increases the voltages necessary to activate this transition decreases (i.e, undesirable reaction is easier at higher temperatures). Ellingham diagram data retrieved from T. B. Reed [9]

Although, KI was considered to be one of the most stable halide candidates, due to its high cost, it was not selected to form an electrolyte. (Table 3.2) Since KBr was shown in Figure 3.1 to be the second most stable candidate halide and possessed a low cost (Table 3.2), it was

selected to form an electrolyte. In addition, KCl was considered to be one of the least stable candidates; however, due its low cost and the fact that successful work had already been demonstrated with LiCl-KCl multi-cation electrolytes in high temperature Li-Al/FeS cells, KCl was also selected to form an electrolyte. [6]

Table 3.2: Commercial Cost for Molten Salt Candidates

Materials	Commercial Prices Researched ($/kilo-mol)
KCl[10]	89.5 - 96.9
LiBr[11]	130 – 261
KBr[12]	142.8 - 357.0
LiCl[13]	42.4 – 424
KI[14]	166-1,660
LiI[15]	63,380

3.2 LiBr-KBr and LiCl-KCl Electrolytes

Shown in Figure 3.2 the composition of the LiBr-KBr electrolyte that was selected for cell operation was (60-40 mol% LiBr-KBr) located at the eutectic. This was to provide the lowest possible melting temperature for the electrolyte.

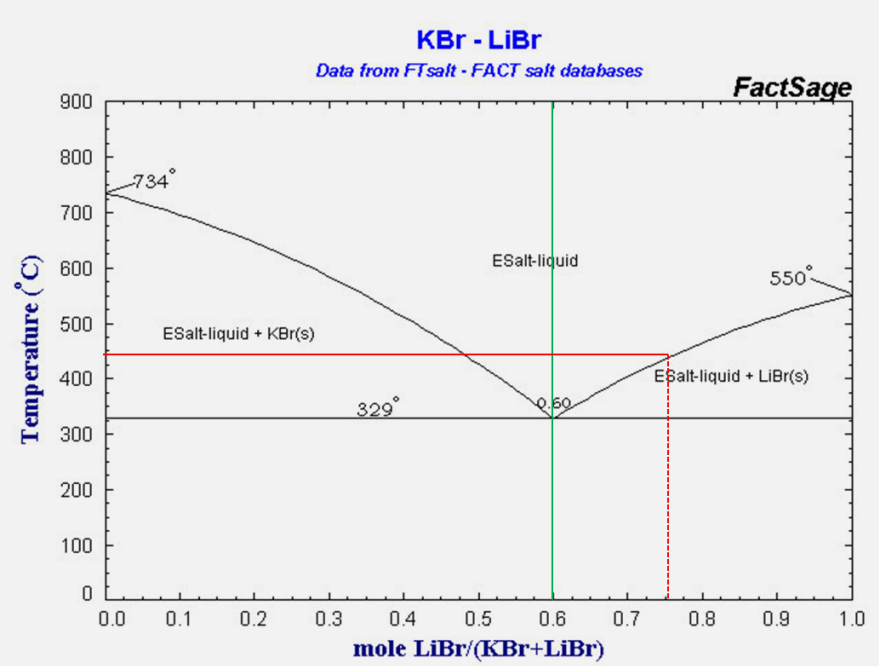

Figure 3.2: The green line depicts the designated composition for the KBr-LiBr electrolyte. The red line reflects the critical composition at which the electrolyte will solidify at 450^0C.[16]

The composition of the LiCl-KCl electrolyte that was selected for cell operation was (67-33 mol% LiCl-KCl), located off-eutectic. (Figure 3.3) This was guided by previous work done on LiCl-KCl in Li-Al/FeS cells at 450^0C that indicated that this composition was critical in achieving a high capacity utilization.[6]

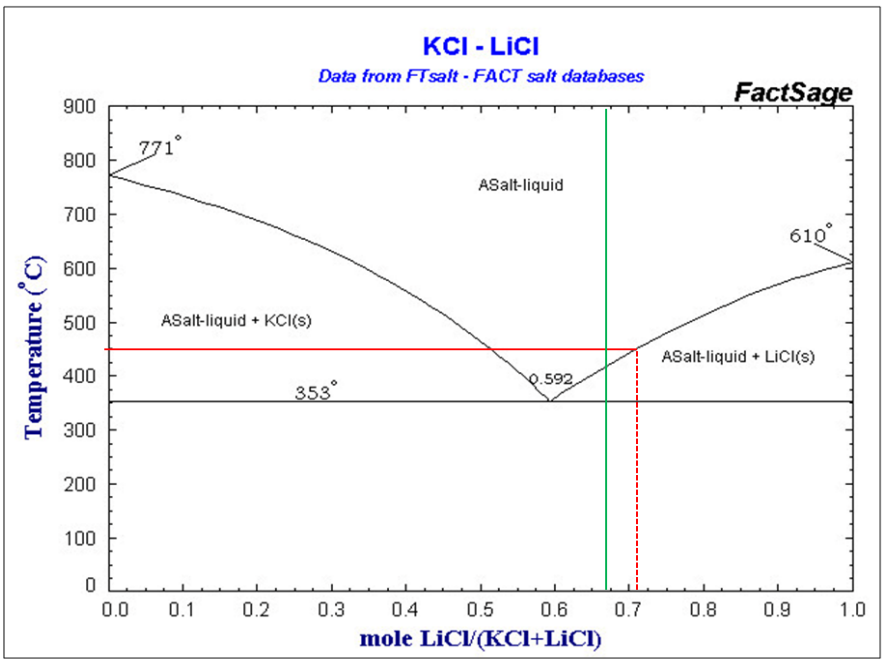

Figure 3.3: The green line depicts the designated composition for the KCl-LiCl electrolyte. The red line reflects the critical composition at which the electrolyte will solidify at 450^0C.[17]

3.3 Multi-cation Electrolyte Selection Summary

The two electrolytes that have been selected for experimentation in this study are LiBr-KBr and LiCl-KCl because of their potential low cost and high electrolyte stability. The LiBr-KBr electrolyte was selected to have a eutectic composition of (60-40 mol% LiBr-KBr) and a melting temperature (~350^0C). In addition, the LiCl-KCl electrolyte was selected to have an off-eutectic composition of (67-33 mol% LiCl-KCl) and a melting temperature (~400^0C). Considerations for possible electrolyte instability in alloy anode LMB systems is that during alloying/dealloying reactions, entropic heat generation or absorption may induce temperature variations at electrode interfaces, potentially leading to sub-melting temperatures. Also, due to ionic concentration polarization established during cycling the electrolyte composition could deviate from the bulk and cause local solidification of the electrolyte. Lastly, the undesirable lithium displacement reaction, where lithium replaces potassium in the electrolyte, could increase the mol% LiCl content in the electrolyte and lead to electrolyte phase instability.

Chapter 4 –KBr-LiBr Electrolyte Functionality in LMBs

4.1 Materials, Test Plan, and Expectations

The active components for this test are shown in Figure 4.1. The purpose of testing the Li-Mg/LiBr-KBr/Sb-Pb system was to confirm, using a Li-Mg alloy anode, that a LiBr-KBr electrolyte can be successfully incorporated in LMBs. In the event of producing a successfully cycling system, it was expected that almost no lithium in the anode would replace potassium in the electrolyte and that almost no potassium would deposit in the cathode. In addition, due to the general trend that the ionic conductivity decreases with decreasing lithium concentration in the electrolyte, shown in Figure 4.2, the ionic conductivity for LiBr-KBr was expected to be less than the conductivity for uni-cation Li^+ salts. Thus, it was expected that higher resistance would be observed in the Li-Mg/LiBr-KBr/Sb-Pb system versus the Li-Mg/LiCl-LiF-LiI/Sb-Pb system when operating at the same conditions. Presented in this study are results of charge/discharge cycling as well as post mortem SEM and EDS analysis.

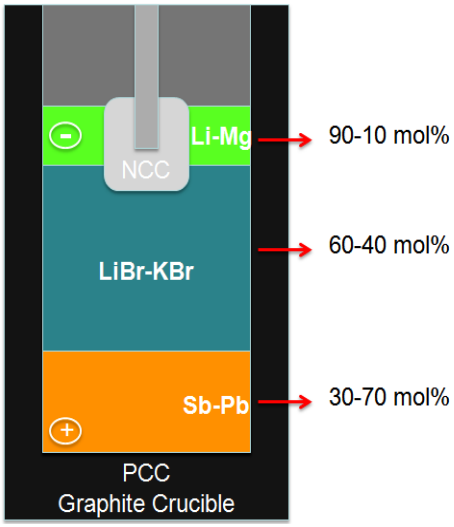

Figure 4.1: Diagram depicts compositions of the active materials within cells tested to confirm Li-Mg anode functionality with LiBr-KBr electrolyte. All active materials were formed using laboratory grade high purity constituents (>99.9% pure).

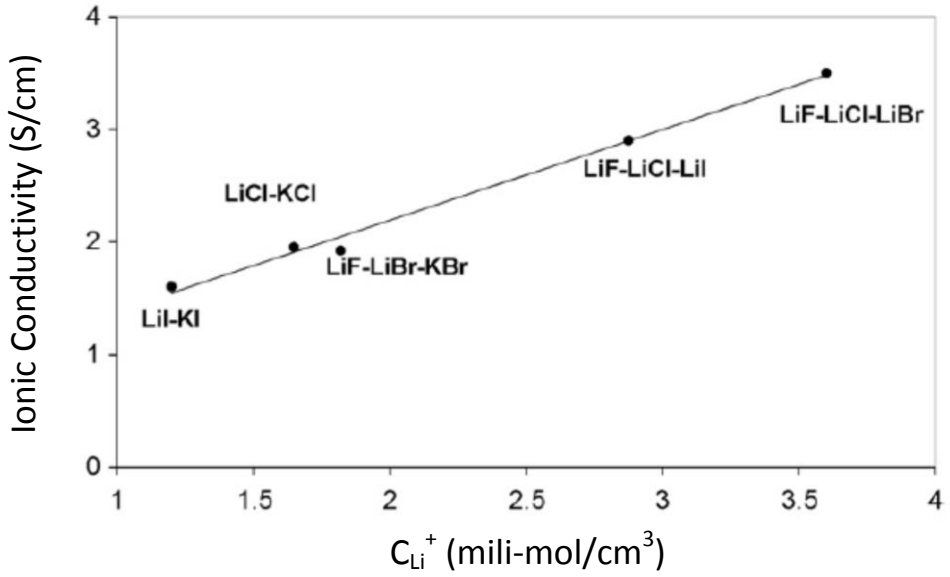

Figure 4.2: Ionic conductivity vs. the lithium concentration in the electrolyte (500^0C). Plot retrieved from Masset. Et al. [3]

4.2 Li-Mg/LiBr-KBr/Sb-Pb Cycling Data

Shown in Figure 4.3, the Li-Mg/LiBr-KBr/Sb-Pb system achieved 75 cycles while maintaining a low and stable resistance profile for a current density of 0.225 A/cm^2 at 440^0C. These results indicate that the electrodes were stable with the electrolyte and no extraneous interactions occurred under these conditions. The resistance for this system at 440^0C and 0.225 A/cm^{2}was observed to be (~0.05 Ohms). This is comparable to the resistance of the Li/LiCl-LiF-LiI/Sb-Pb system at 450^0C and 0.275 A/cm^{2}which is typically (~0.03 Ohms).

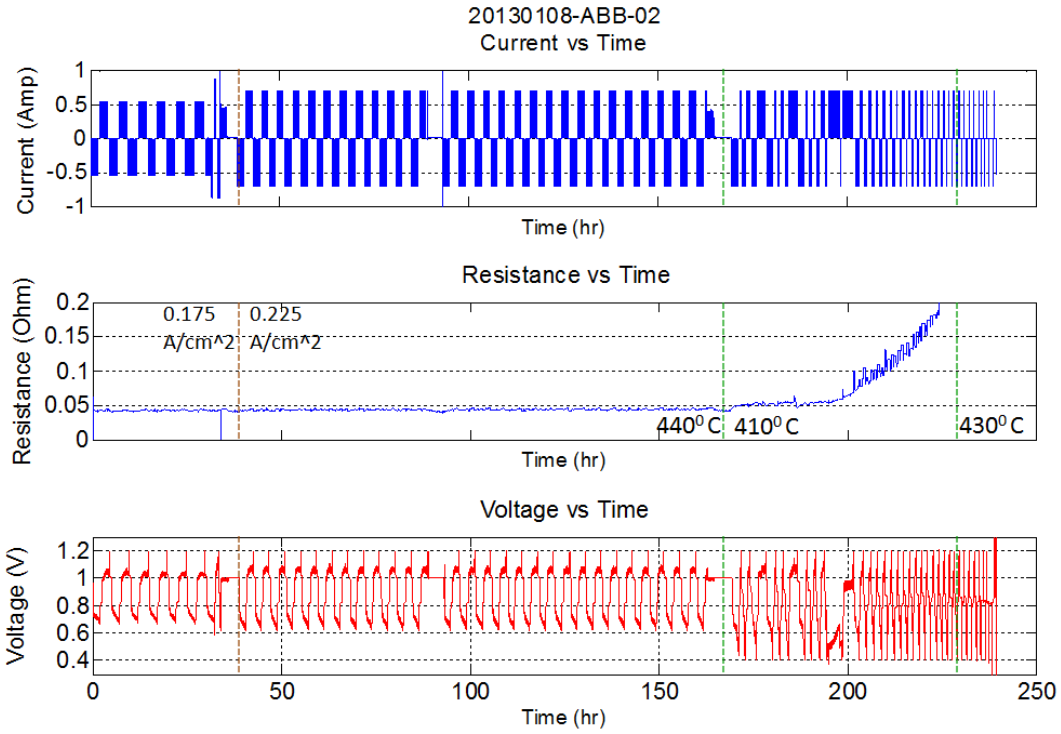

Figure 4.3: Depicts current, resistance, and voltage profiles for Li-Mg/LiBr-KBr/Sb-Pb cell. Green dashed lines represent where temperature transitions occur and brown dashed lines represent current transitions.

As shown in Figure 4.4 (A), the Li-Mg/LiBr-KBr/Sb-Pb system was capable of maintaining an energy efficiency of 62% and columbic efficiency of 98% for a current density of 0.225 A/cm^{2}at 440^{0}C. In addition, Figure 4.4 (B) confirms, for the same conditions, that this cell consistently achieved 91% theoretical capacity when discharging and 93% theoretical capacity when charging per cycle. However, at a current density of 0.275 A/ cm^2, shown in Figure 4.5, the Li-Mg/LiBr-KBr/Sb-Pb system was observed to exhibit irregular voltage profiles.

(A) (B)

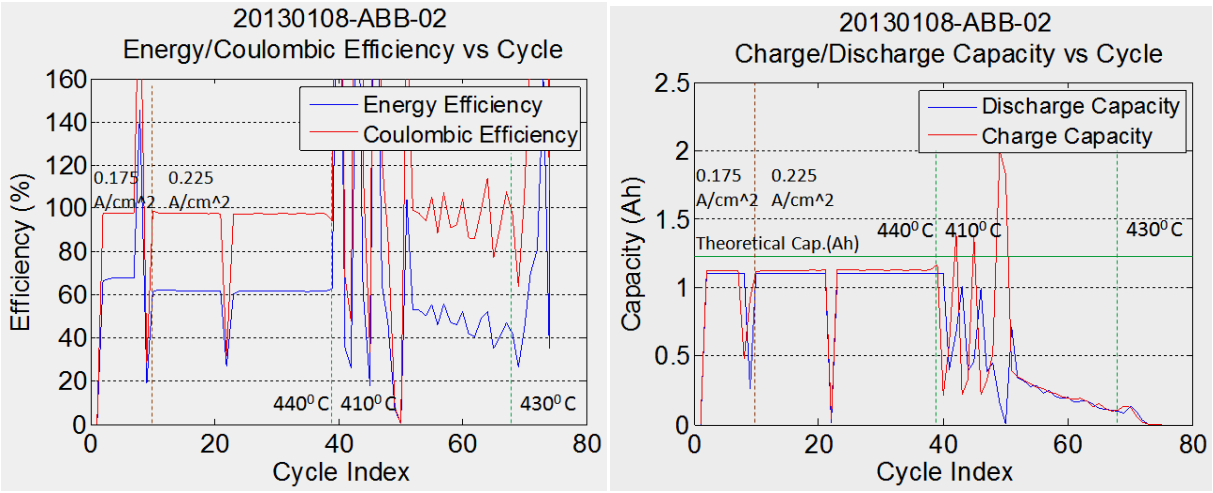

Figure 4.4: For both plots the green dashed lines mark temperature transitions while the brown dashed lines mark current transitions. In addition, it is important to note that the downward spike in efficiency and drop in capacity around 7 cycles is due to a very brief increase in current from 0.175 A/cm^{2}to 0.225 A/cm^2. (A) Depicts the energy and coulombic efficiency for the Li-Mg/LiBr-KBr/Sb-Pb system over a range of temperatures and currents. (B) Depicts the capacity utilization per cycle for the Li-Mg/ LiBr-KBr/Sb-Pb system over a range of temperatures and currents. Theoretical capacity is labeled with a solid green line. Spikes in the plot that reach zero (Ah) correlate to moments where leakage current measurements were taken.

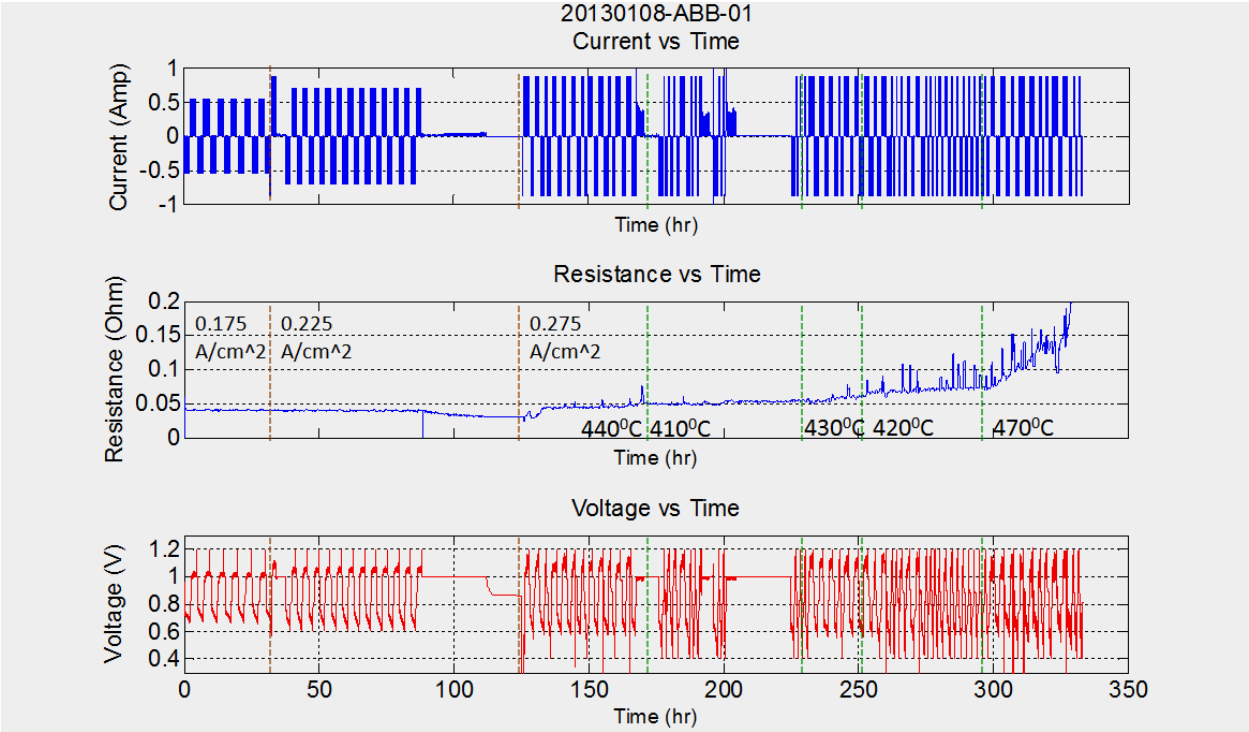

Figure 4.5: Depicts current, resistance, and voltage data for Li-Mg/LiBr-KBr/Sb-Pb cell. Green dashed lines represent where temperature transitions occur and brown dashed lines represent current transitions.

Moreover, resistance fluctuations and unstable voltage profiles were observed with the temperature transition from 440^0C to 410^0C shown in Figure 4.3. The gradual rise in resistance and degradation of the voltage profile associated with this temperature transition may be attributed to the fact that operating at 410^0C caused the Li-Mg anode to enter into the solid phase region. Additional experiments are needed to identify detailed mechanisms of failure. Shown in Figure 4.6, at 410^0C the low lithium content Li-Mg alloy that is present on complete discharge (70-30 mol% Li-Mg) is almost on the border of the solid phase transition.

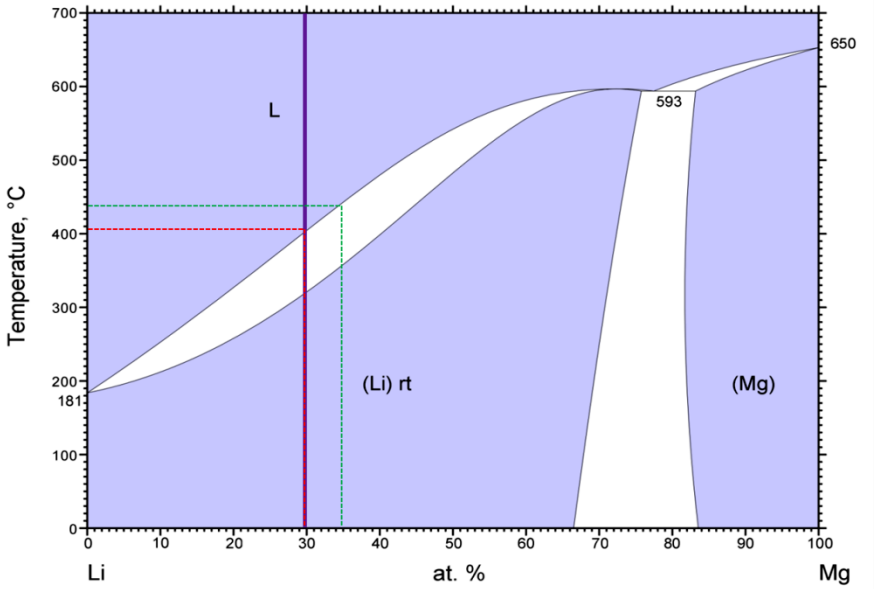

Figure 4.6: The purple line corresponds to the anode composition upon full discharge. The red and green lines refer to the critical compositions at which the Li-Mg anode will solidify at 410^0C and 440^0C respectively. Phase diagram retrieved from Kevorkov D.G.[8]

The voltage profile associated with the Li-Mg/LiBr-KBr/Sb-Pb system for a current density of 0.225 A/cm^{2}can be observed in Figure 4.7 where the charge voltage is (~0.09V) larger than the standard cell's (Li/LiCl-LiF-LI/SbPb) charge profile and the discharge voltage is (~0.07 V) smaller than the standard cell's discharge profile. The potential penalties for the LiBr-KBr system, already occurring at a lower current density of 0.225 A/cm^2 when compared to the

standard cell at 0.275 A/cm2, are expected due to use of a Li-Mg alloy anode and the fact that the LiBr-KBr electrolyte possess a lower conductivity than the Li^+ uni-cation electrolytes. (Figure 4.2)

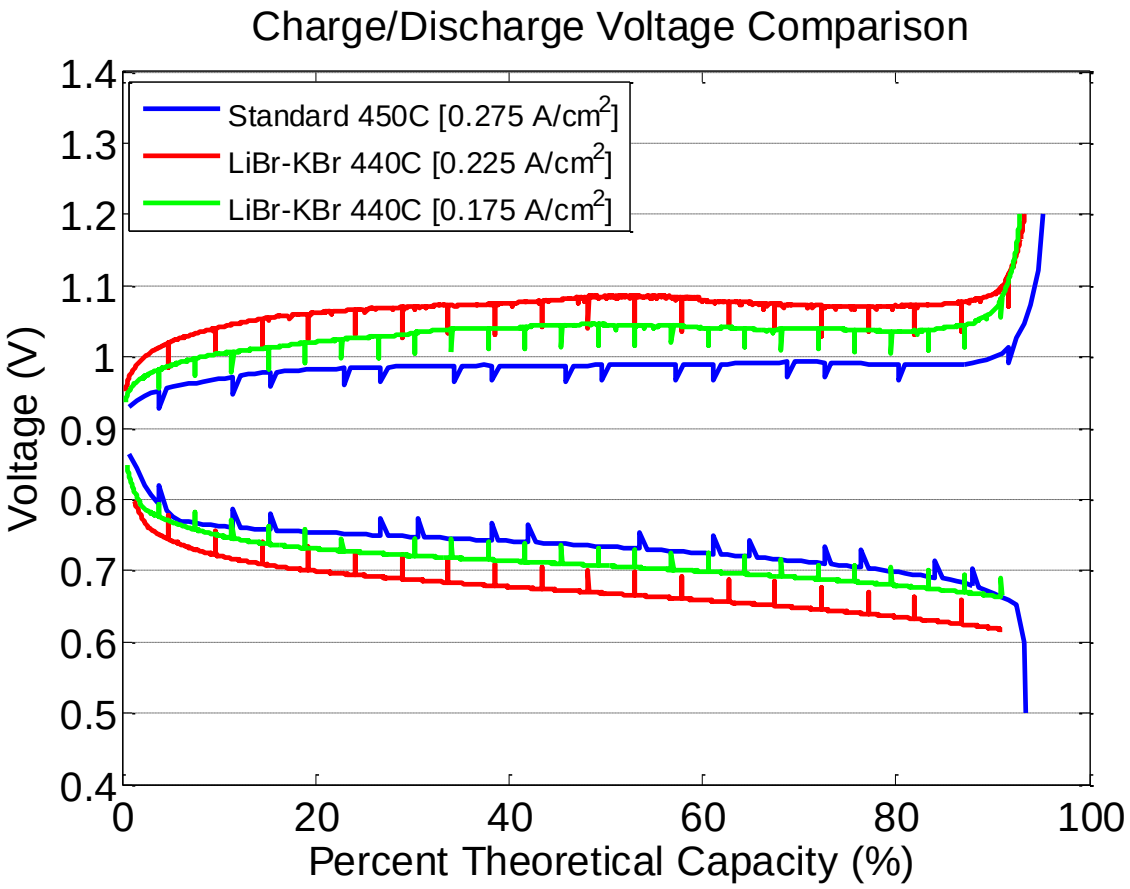

Figure4.7: Depicts voltage (V) versus percent theoretical capacity (%) for the Li/LiCl-LiF-LiI/Sb-Pb system labeled standard and the Li-Mg/LiBr-KBr/Sb-Pb system labeled LiBr-KBr with their respective testing conditions. The spikes correspond to instances where resistance measurements were taken.

4.3 Li-Mg/LiBr-KBr/Sb-Pb Post-Mortem Analysis

Cell 20130108-ABB-02 experienced periodic spikes in resistance that lead to cell failure while in the discharged state. (Figure 4.2) Cell 20130108-ABB-01, shown in Figure 4.8 (A), and cell 20130108-ABB-02, shown in Figure 4.8 (B), were both observed to have lost a significant amount of electrolyte. The phenomenon of electrolyte seeping out of the base of the graphite

crucible has been observed for cells of various chemistries, including the Li/LiCl-LiF-LiI/Sb-Pb system. (Figure 4.9) In many instances, cells possessing a longer cycle life or consistent resistance fluctuations tended to experience more pronounced seepage. (Figure 4.9) Moreover, cell 20130108-ABB-01 experienced similar phenomenon in resistance spikes as cell 20130108-ABB-02 and possessed similar efficiencies. SEM and EDS was performed on cell 20130108-ABB-01 shown in Figures 4.10 and 4.11.

(A) (B)

20130108-ABB-01 **20130108-ABB-02**

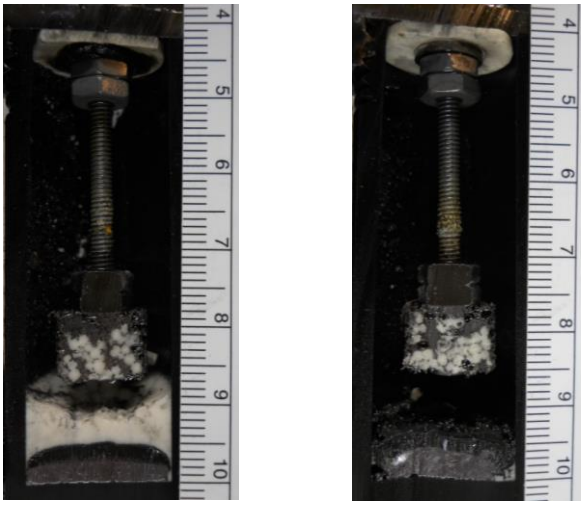

Figure 4.8: Depicts post mortem pictures of two cells which were terminated in the discharge state, ruler is in units of centimeters. (A) Cell 20130108-01 still has electrolyte left in its PCC crucible although a noticeable portion appears to have left the cell (B) Cell 20130108-ABB-02 only has electrolyte trapped in the NCC.

Figure 4.9: Depicts a batch of four 20121202 Li-Mg/LiCl-KCl/Sb-Pb cells ordered 1-4 from left to right. Cells 01 and 02 cycled longer and observed regular resistance spikes, cell 03 did not cycle as long, and cell 04 suffered from a connection failure not cycling at all.

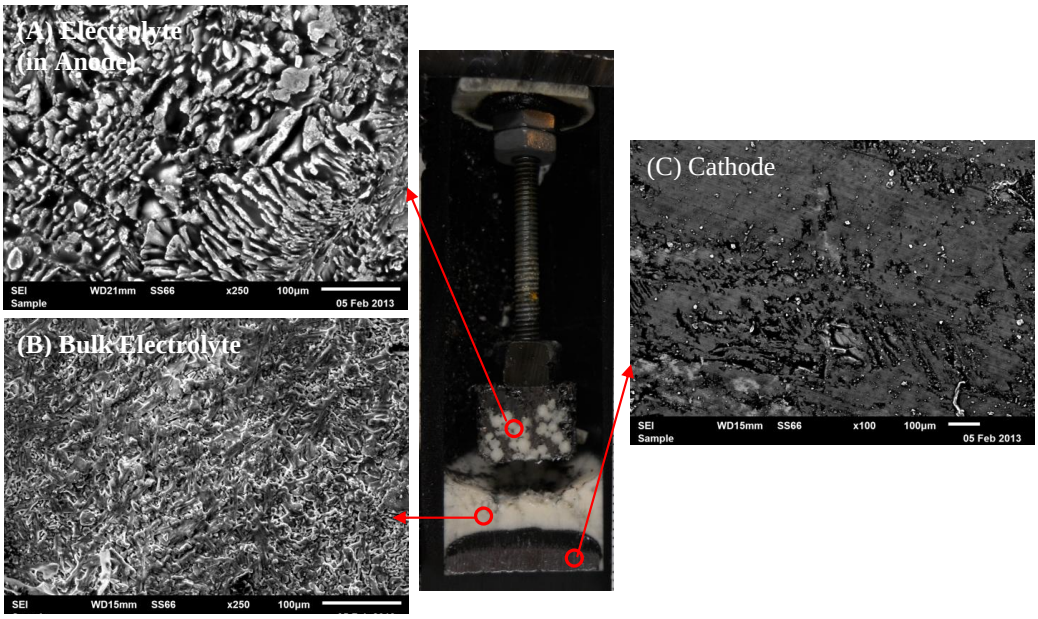

Figure 4.10: Depicts SEM images for (A)Electrolyte in the anode, (B) Bulk electrolyte, and (C) Cathode. A scale bar is located at the lower right edge of each picture. The corresponding values associated with the scale bars are (A) 100µm (B) 100µm and (C) 100µm.

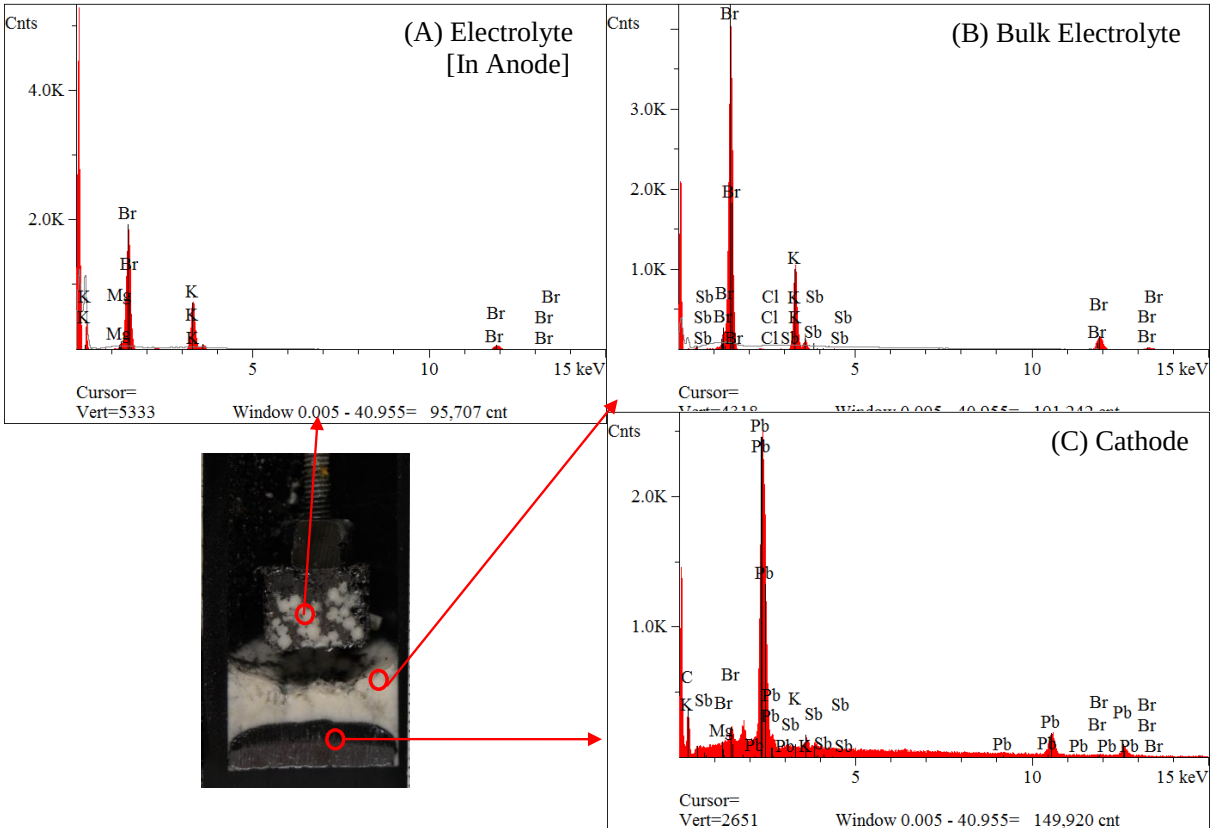

Figure 4.11: Depicts EDS plots output for (A)Electrolyte in the anode, (B) Bulk electrolyte and (C) Cathode regions of the cell at 20.0 kV and a 35^0 takeoff angle. Plots correspond to SEM images in Figure 4.10. The elapsed livetime values associated with each plot is (A) 23.5 (B) 26.1 and (C) 28.5.

Due to the fact that the anode of cell 20130108-ABB-01 was primarily filled with electrolyte, it was very difficult to observe a portion of the anode that contained any alloy. (Figure 4.8 (A)) Thus, SEM and EDS was done on the electrolyte trapped in the anode of the cell. This electrolyte was found to be composed of 47.5% potassium and 52.5% bromine. (Table 4.1) This indicates that the electrolyte in the anode is composed mostly of the KBr halide.

Table 4.1: EDS Data for ELC in Anode, Bulk ELC, Dark ELC, Intermetallic, and Cathode

Elements	ELC in Anode Composition (Atomic %)	Bulk ELC Composition (Atomic %)	Cathode Composition (Atomic%)	Intermetallic Composition (Atomic %)
Magnesium	0.0	0.1	1.6	(Protected)
Iron	-	-	-	(Protected)
Potassium	47.5	32.5	0.7	2.7
Bromine	52.5	66.9	5.6	(Protected)
Chlorine	-	0.2	-	(Protected)
Lead	-	-	82.0	(Protected)
Antimony	-	0.3	10.1	(Protected)
	100	100	100	100

The designated electrolyte composition was 60-40 mol% LiBr-KBr. The post-mortem composition of the bulk electrolyte in atomic% was found to be 66.9% bromine and 32.5% potassium shown in Table 4.1. This closely corresponds with the designated composition of the electrolyte; however, a slightly higher than expected KBr concentration was observed. Moreover, the composition of the cathode was designated to be 30-70 mol% antimony-lead. Post-mortem, the ratio of antimony to lead in the cathode was found to be 11-99 atomic%. This composition differs from the designated composition and indicates that regions of high lead concentration exist in the bulk cathode. Other constituent elements that were detected in the cathode aside from

antimony and lead are most likely due to electrolyte contamination due to EDS sample preparation.

Furthermore, shown in Figure 4.11, there are no clearly observable peaks for potassium in the cathode of the cell. In addition, EDS analysis done on both the cathode and the intermetallic region above the cathode conveyed that traces of potassium in these regions were very small (< 3%) and most likely negligible given EDS detection limits as well as sample preparation. (Table 4.1) This indicates that the LiBr-KBr electrolyte is stable with the cathode of the cell. Further studies may be needed to identify the cause of electrolyte loss.

4.4 **Li-Mg/LiBr-KBr/Sb-Pb LMB Functionality Summary**

The Li-Mg/LiBr-KBr/Sb-Pb system achieved over 70 cycles demonstrating energy efficiencies of 62% and columbic efficiencies of 98% for a current density of 0.225 A/cm^{2}at 440^{0}C. In addition, the LiBr-KBr electrolyte was verified with aid of EDS and SEM to be stable with the cathode and intermetallic components of the cell post-mortem. Moreover, this cell failed to operate at low temperatures (~410^{0}C) indicated by resistance spikes and fluctuating voltage profiles associated with this temperature transition. This is believed to be attributed to a possible solid phase transition in the anode at (~410^{0}C).

Chapter 5 –KCl-LiCl Electrolyte Functionality in LMBs

5.1 Materials, Test Plan, and Expectations

The active components for this test are shown in Figure 4.1. The purpose of testing the Li-Mg/LiCl-KCl/Sb-Pb system was to confirm, using a Li-Mg alloy anode, that a LiCl-KCl electrolyte can be successfully incorporated in LMBs. In the event of producing a successfully cycling system, it was expected that almost no lithium in the anode would replace potassium in the electrolyte and that almost no potassium would deposit in the cathode. In addition, it is important to note that the ionic conductivity for the LiCl-KCl electrolyte at (~500^{0}C) is 1.57 S/cm^2 which is much less than conductivity of Li^+ uni-cation electrolytes at similar temperatures (~3 S/cm^2). (Figure 4.3) This results in larger overpotential values and higher resistance values observed in the Li-Mg/LiCl-KCl/Sb-Pb system versus the Li-Mg/LiCl-LiF-LiI/Sb-Pb system when operating under the same conditions. Presented in this study are results of charge/discharge cycling as well as post-mortem SEM and EDS analysis.

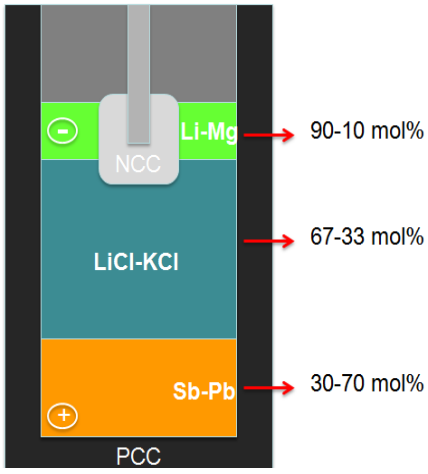

Figure5.1: Describes compositions of the active materials within cells tested to confirm Li-Mg anode functionality with LiCl-KCl electrolyte. All active materials were formed using high purity constituents (>99.9%

5.2 Li-Mg/LiCl-KCl/Sb-Pb Cycling Data

The Li-Mg/LiCl-KCl/Sb-Pb system was demonstrated to achieve over 75 cycles. (Figure 5.2 (A)) In addition, the Li-Mg/LiCl-KCl/Sb-Pb system was capable of maintaining an energy efficiency of 67% and columbic efficiency of 97% when operating at a current density of 0.175 A/cm^2 and temperature of 490^{0}C. (Figure 5.2 (A)) Also, for the same conditions, this cell consistently achieved 87% theoretical capacity when discharging and 92% theoretical capacity when charging per cycle. (Figure 5.2 (B))

(A) (B)

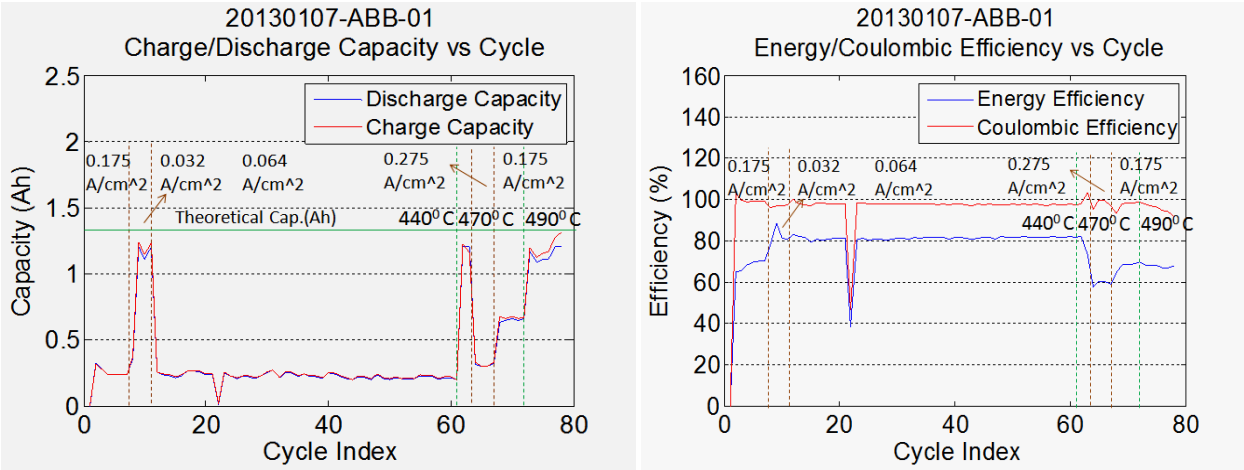

Figure 5.2: For both plots the green dashed lines mark temperature transitions while the brown dashed lines mark current transitions. (A) Depicts the energy and coulombic efficiency for the Li-Mg/LiCl-KCl/Sb-Pb system over a range of temperatures and currents. Drastic spike in this plot corresponds to leakage current measurement. (B) Depicts the capacity utilization per cycle for the Li-Mg/ LiCl-KCl/Sb-Pb system over a range of temperatures and currents. Theoretical capacity is labeled with a solid green line. Spikes in the plot that reach zero (Ah) correlate to moments where leakage current measurements were taken.

Temperature was found to be a critical factor in allowing Li-Mg/LiCl-KCl/Sb-Pb cells to achieve a stable resistance profile and high capacity utilization. Depicted in Figure 5.3, regular resistance spikes were observed for current densities of 0.032 A/cm^2, 0.064 A/cm^2, and 0.175 A/cm^{2}at 440^{0}C. In addition, at 440^{0}C, the charge/discharge theoretical capacity utilizations were

(~15%) corresponding with current densities of 0.064 A/cm^2 and 0.175 A/cm^2. (Figure 5.2 (A)) When the temperature was shifted to 470^{0}C there were no observable resistance spikes for any of the current densities stated above and cells operating at 0.064 A/cm^{2}were observed to achieve ~90% capacity utilization when charging and discharging. (Figure 5.3 and Figure 5.2 (A)) A further increase in temperature to 490^{0}C allowed cells operating at 0.175 A/cm^{2}to achieve ~90% capacity utilization. (Figure5.2 (A)) The resistance at 490^{0}C was observed to be (~0.05 Ohms) which is comparable to the resistance of the Li/LiCl-LiF-LiI/Sb-Pb system at 450^{0}C and 0.275 A/cm^2, typically (~0.03 Ohms).

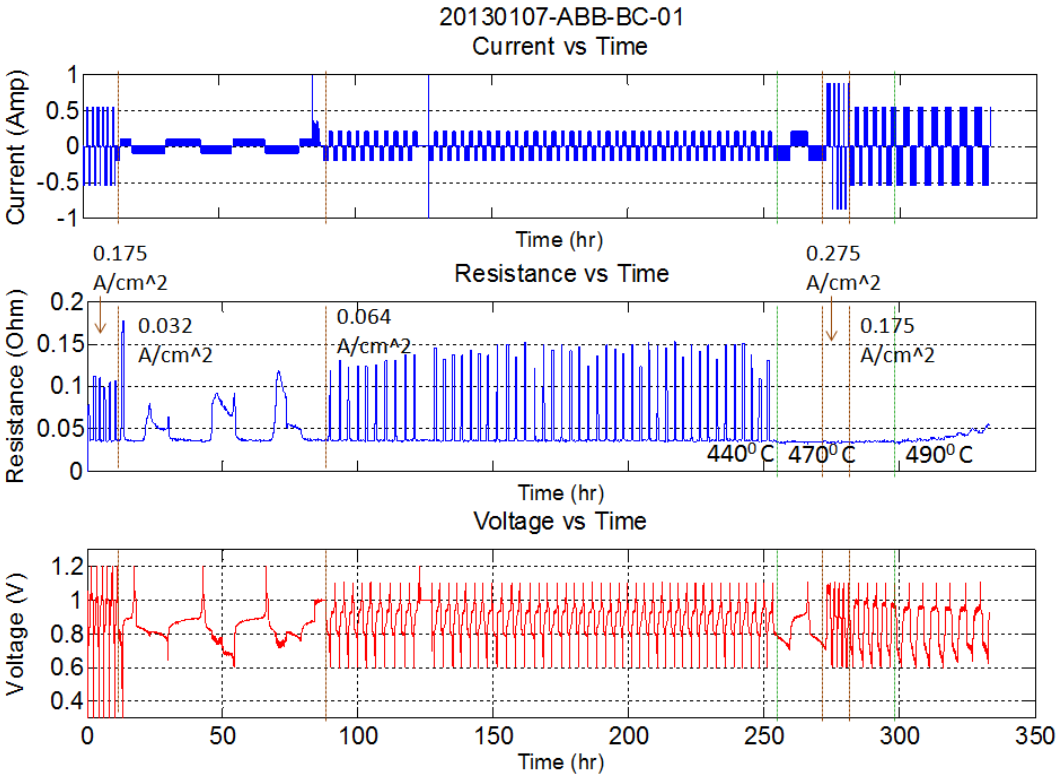

Figure 5.3: Depicts current, resistance, and voltage data for Li-Mg/LiCl-KCl/Sb-Pb cell. Green dashed lines represent where temperature transitions occur and brown dashed lines represent current transitions.

At 440^{0}C for the Li-Mg/LiCl-KCl/Sb-Pb system a very small change in the composition by route of increased mol% LiCl was shown in Figure 5.4 to make the LiCl-KCl electrolyte prone to solidification. This liquid to solid phase change in the electrolyte may account for the

observed resistance spikes, shown in Figure 5.3, and the poor capacity utilization at 440^0C. A mechanism that accounts for this phenomenon is the ionic concentration polarization established during cycling. This may cause deviation from the bulk concentration and cause local solidification of the electrolyte. Additionally, during alloying/dealloying reactions, entropic heat generation or absorption may also induce temperature variations at electrode interfaces potentially leading to sub-melting temperatures. Another possibility is the undesirable lithium displacement reaction, where lithium replaces potassium in the electrolyte, increases the mol% LiCl content in the electrolyte. Shown in Figure 5.5, when increasing the temperature and keeping the current density constant, the capacity utilization increases dramatically. This would correlate well with the fact that at higher temperatures a liquid to solid phase transition in the electrolyte is less prone to occur.

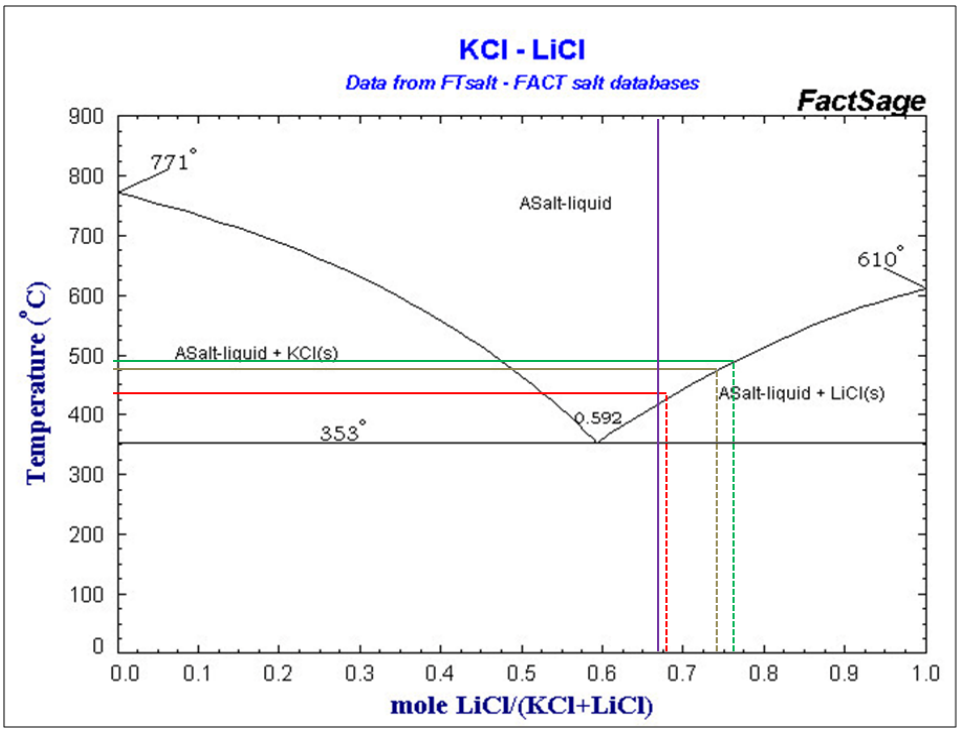

Figure 5.4: The purple line corresponds to the designated electrolyte composition for the Li-Mg/LiCl-KCl/Sb-Pb system. The red, gold, and green lines refer to the critical compositions at which the electrolyte will solidify at 440^0C, 470^0C, and 490^0C respectively.[17]

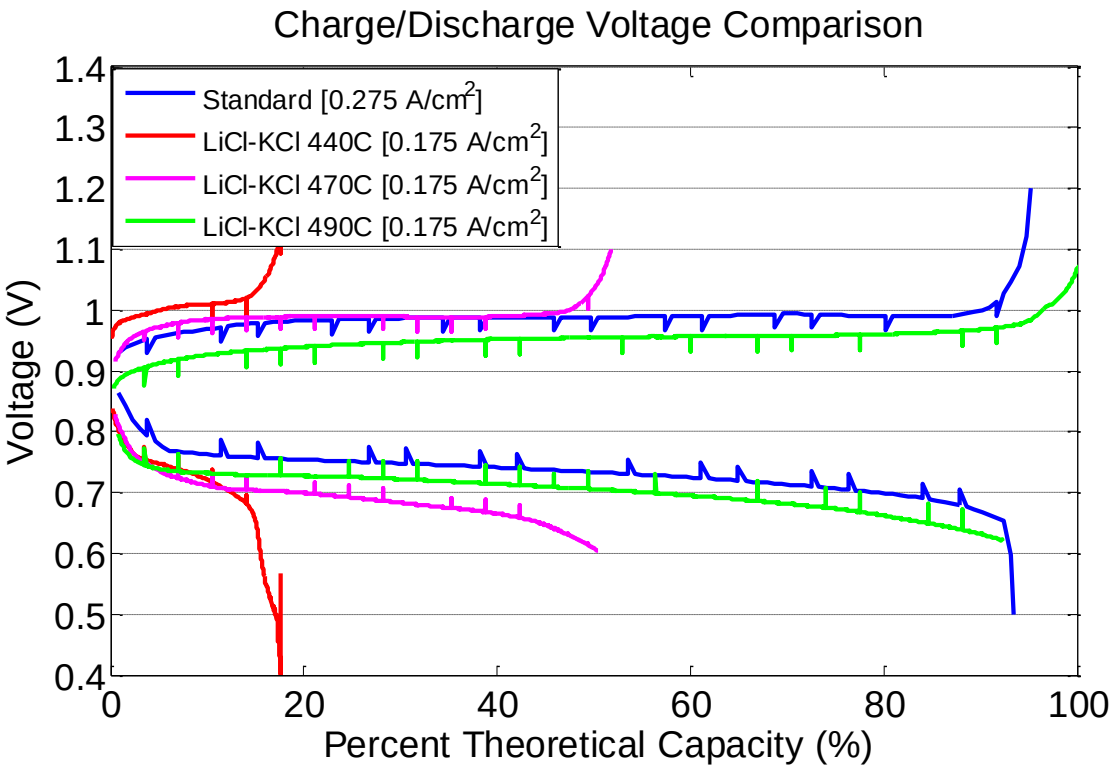

Figure 5.5: The Li/LiCl-LiF-LiI/Sb-Pb system is labeled standard and the Li-Mg/LiCl-KCl/Sb-Pb system is labeled LiCl-KCl with its respective testing conditions. The spikes correspond to instances where resistance measurements were taken.

5.3 Li-Mg/LiCl-KCl/Sb-Pb Post-Mortem Analysis

Post-mortem pictures of cell 20130107-ABB-01 and cell 20130107-ABB-03 are shown in Figure 5.6. Cell 20130107-ABB-03 was cycled at 0.032 A/cm^{2}for the duration of its cycle life and experienced similar phenomenon in resistance spikes and efficiencies when compared to cell 20130107-ABB-01 operating at the same conditions. At temperatures at or above 470^{0}C these resistance spikes were observed to disappear in cell 20130107-ABB-03 as was the case for cell 20130107-ABB-01. SEM and EDS was performed on cell 20130108-ABB-03 shown in Figures 5.7 and 5.8.

(A) (B)

20130107-ABB-01 20130107-ABB-03

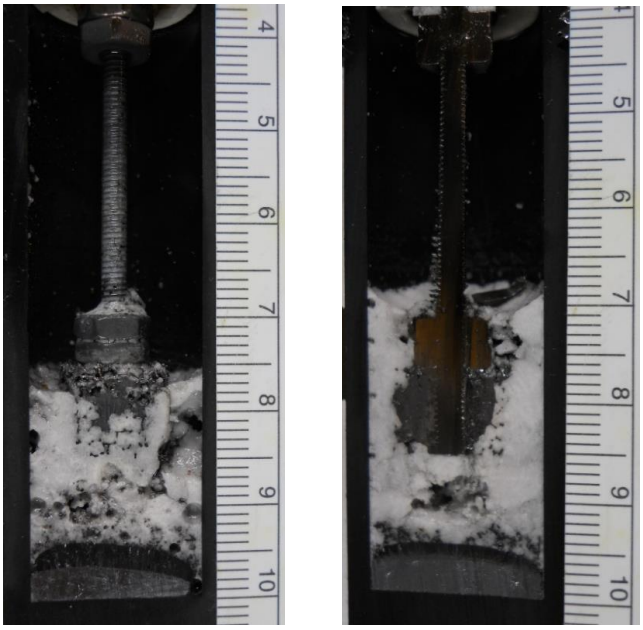

Figure 5.6: Depicts the post mortem pictures two cells, scale is in units of cm. (A) Manually stopped cycling while in discharge state, (B) Manually stopped cycling while in the middle of the charged state.

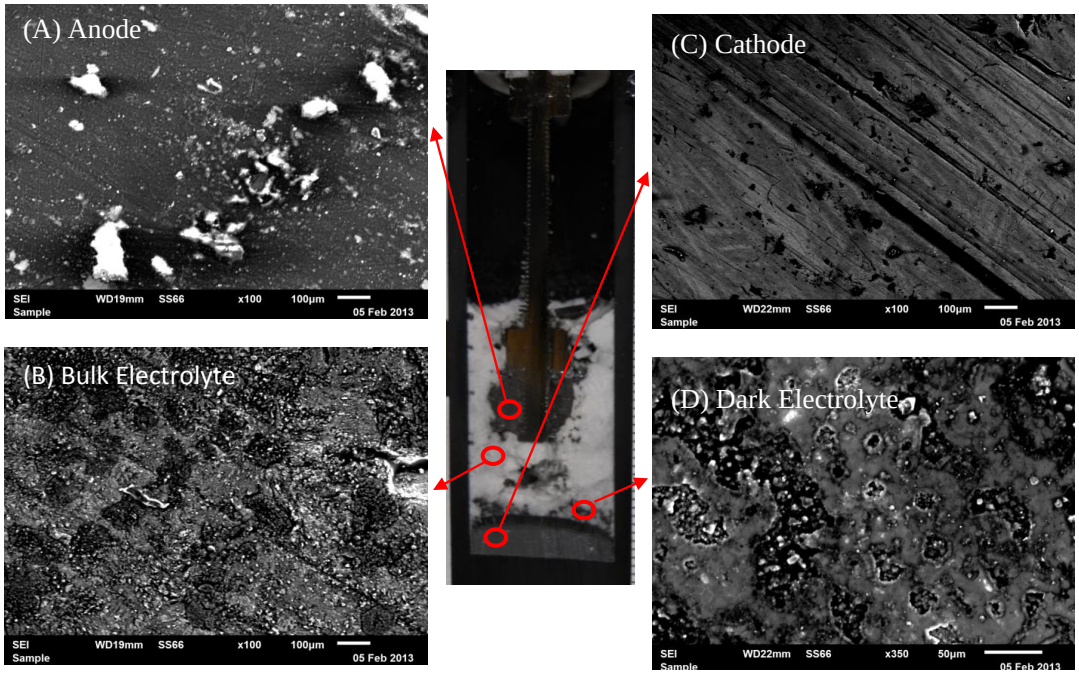

Figure 5.7: Depicts SEM images for (A) Electrolyte in the anode, (B) Bulk electrolyte, (C) Cathode, and (D) Dark electrolyte shown from left to right. A scale bar is located at the lower right edge of each picture. The corresponding values associated with the scale bars are (A) 100 µm (B) 100 µm (C) 100 µm and (D) 50 µm.

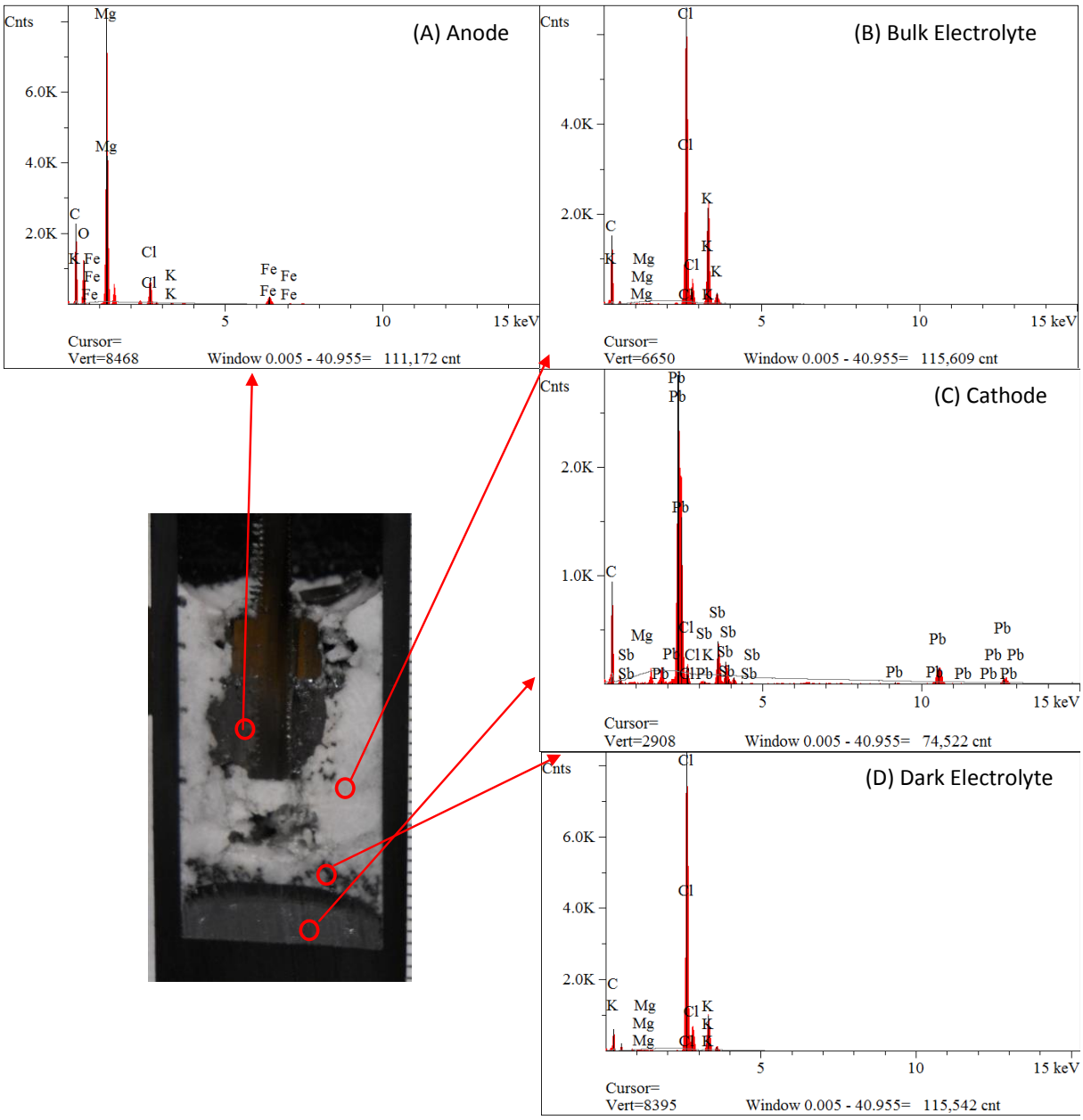

Figure 5.8: Depicts EDS plots output for (A)Electrolyte in the anode, (B) Bulk electrolyte, (C) Cathode, and (D) Dark electrolyte regions of the cell at 20.0 kV and a 35^0 takeoff angle. Plots correspond to SEM images in Figure 5.7. The elapsed livetime values associated with each plot is (A) 73.7 (B) 45.9 (C) 50.2 and (D) 54.3.

The designated anode composition was 90-10 mol% lithium-magnesium in the charge state. Due to EDS detection limits, lithium could not be detected; however; the post-mortem composition of the anode was found to be primarily magnesium (84.5%), iron (which comprises

the negative current collector), and what is most likely electrolyte contaminants present due to EDS sample preparation, explained further in section 1.3. (Table 5.1) Thus, the results in Table 5.1 match with what was expected to comprise the anode.

Table 5.1: EDS Data for Anode. Bulk ELC. Dark ELC. Intermetallic. and Cathode

Elements	**Anode Composition (Atomic %)**	**Bulk ELC Composition (Atomic %)**	**ELC Near Intermetallic Composition (Atomic %)**	**Cathode Composition (Atomic%)**	**Intermetallic Composition (Atomic %)**
Magnesium	84.5	0.5	0.8	1.6	2.1
Iron	5.6	-	-	-	(Protected)
Potassium	0.8	34.6	17.3	0.2	2.0
Chlorine	9.1	64.9	81.9	4.7	(Protected)
Lead	-	-	-	59.7	(Protected)
Antimony	-	-	-	33.8	(Protected)
	100	100	100	100	100

The designated electrolyte composition was 67-33 mol% LiCl-KCl which constitutes a 33 mol% ratio of potassium to chlorine. The ratio of potassium to chlorine found in the bulk electrolyte post-mortem was (~53 atomic%). This conveys that a higher KCl content electrolyte was observed post-mortem compared to the composition originally designated. Regarding the "dark electrolyte", which refers to the layer of electrolyte closest to the intermetallic, post-mortem, it was found that the ratio of potassium to chlorine was 21%. (Table 5.1) Thus, the dark electrolyte region was observed to have a slightly lower than expected KCl halide content post-mortem. It is possible that a low content KCl, or high content LiCl, electrolyte forms near the intermetallic layer and encourages the electrolyte to solidify in this region at lower temperatures (~440^0C).

Moreover, the composition of the cathode was designated to be 30-70 mol% antimony-lead. Post-mortem, the ratio of antimony to lead was found to be 36-64 atomic%. This corresponds very well to the designated composition of the cathode. (Table 2.1) Other

constituent elements that were detected in the cathode aside from antimony and lead are most likely due to electrolyte contamination due to EDS sample preparation.

Furthermore, shown in Figure 5.8 there are no clearly observable peaks for potassium in the cathode or anode of the cell. In addition, EDS analysis performed on the anode, cathode, and intermetallic regions of the cell conveyed that traces of potassium in these regions were very small ($\leq$ 2%) and most likely negligible given EDS detection limits and sample preparation. (Table 4.1) This indicates that the LiCl-KCl electrolyte is stable with the cathode of the cell.

5.4 **Li-Mg/LiCl-KCl/Sb-Pb LMB Functionality Summary**

The Li-Mg/LiCl-KCl/Sb-Pb system achieved over 75 cycles demonstrating energy efficiencies of 67% and columbic efficiencies of 97% at 490^0C and 0.175 A/cm^2. In addition, the LiCl-KCl electrolyte was verified with aid of EDS and SEM to be stable with the cathode and anode components of the cell. Temperature was found to be a critical factor in achieving a stable resistance profile and high capacity utilization. This is most likely due to the fact that the LiCl-KCl off-eutectic electrolyte is susceptible to solidification at lower temperatures and high current densities. At lower temperatures (~440^0C) small fluctuations in the LiCl content of the electrolyte could spark a liquid to solid phase transition. (Figure 5.4) In addition, previous work has demonstrated for molten multi-cation electrolytes (e.g., LiCl-KCl eutectic) that, at high current densities, concentration polarization can result in the formation of solids at the electrode interfaces due to electrolyte composition shifts.[3] These findings convey that it is not possible for this system to operate at current densities above 0.175 A/cm^2 at temperatures significantly below (~490^0C) without suffering from poor cell performance.

Chapter 6 – Battery Cost Analysis

Cost was a major driver in deciding which chemistries would compose the different batteries that were tested in this study. Having demonstrated successful cyclability for the Li-Mg/LiBr-KBr/Sb-Pb and Li-Mg/LiCl-KCl/Sb-Pb systems it was necessary to analyze the potential cost reductions associated with these cells. To convey impact in cost reduction, information on the cost of one of the lowest cost LMB systems currently developed, BatteryAlpha (Li/electrolyte/Sb-Pb), was utilized in this section. All cost figures were based on price of commercial grade materials. (Table 6.1)

Table 6.1: Material Prices for Cost Model

Materials	Commercial Prices Researched ($/kilo-mol)	*Prices Used in Model ($/kilo-mol)
Li[18]	428	428
Mg[18]	69	69
Sb[18]	1,770	1,770
Pb[18]	520	520
KI[14]	166-1,660	913
KBr[12]	142.8 - 357.0	249.9
KCl[10]	89.5 - 96.9	93.2
LiI[15]	63,380	63,380
LiBr[11]	130 – 261	195.5
LiCl[13]	42.4 – 424	233.2
LiF[19]	25.94 - 259.4	142.67
NaCl[20]	2.9– 5.8	4.4
NaF[21]	32.8	32.8

*The prices used in the this cost model were derived by averaging the price ranges based on the assumption that large scale production would require the purchasing of bulk quantities which would reduce the asking price.

6.1 **Li-Mg/LiBr-KBr/Sb-Pb Cost Analysis**

This cost model was based on performance metrics of cell 20130108-ABB-02 operating at 440^0C and 0.225A/cm^2, assuming that the NCC was designed to store an equivalent capacity as BatteryAlpha. The cost data in Table 6.1 and the active material data in Table 6.2 were used to calculate the energy cost of the active materials in the cell, shown in Table 6.3.

Table 6.2: Active Materials Cost per Cell (Li/LiBr-KBr/Sb-Pb)

Active Materials in Li/LiBr-KBr/Sb-Pb	**Active materials per cell (mili-mols)**	**Active Materials Cost per cell ($)**
Li	95.4	0.0408
Mg	10.6	0.0007
Sb	25.9	0.0458
Pb	60.47	0.0314
LiBr	120	0.0235
KBr	80.2	0.0200
	Sum	0.1624

Table 6.3: Energy and Power Cost per Cell (Li-Mg/LiBr-KBr/Sb-Pb)

	Li-Mg/LiBr-KBr/Sb-Pb
Avg. Charge/Discharge Time (hrs)	2.72
Avg. Discharge Voltage (V)	0.66
Avg. Discharge Capacity (Ah)	1.72
Energy Cost for Cathode ($/kWh)	68
Energy cost for Anode ($/kWh)	36
Energy Cost of LiBr-KBr ELC ($/kWh)	38
Energy Cost for Active Materials ($/kWh)	142
Power Cost for Active Materials ($/kW)	386

6.2 **Li-Mg/LiCl-KCl/Sb-Pb Cost Analysis**

This cost model was based on performance metrics of cell 20130107-ABB-01 operating at 490^0C and 0.175A/cm^2, assuming that the NCC was designed to store an equivalent capacity as BatteryAlpha. The cost data in Table 6.1 and the active material data in Table 6.4 were used to calculate the energy cost off the active materials in the cell, shown in Table 6.5.

Table 6.4: Active Materials Cost per Cell (Li/LiCl-KCl/Sb-Pb)

Active Materials in Li/LiCl-KCl/Sb-Pb	**Active materials per cell (mili-mols)**	**Active Materials Cost per cell ($)**
Li	95.4	0.428
Mg	10.6	0.069
Sb	25.9	1.77
Pb	60.47	0.52
LiCl	190	0.2331
KCl	94.3	0.0932
	Sum	0.1719

Table 6.5: Energy and Power Cost per Cell (Li-Mg/LiCl-KCl/Sb-Pb)

	Li-Mg/LiCl-KCl/Sb-Pb
Avg. Charge/Discharge Time (hrs)	3.56
Avg. Discharge Voltage (V)	0.69
Avg. Discharge Capacity (Ah)	1.7
Energy Cost for Cathode ($/kWh)	66
Energy cost for Anode ($/kWh)	35
Energy Cost of LiCl-KCl ELC ($/kWh)	45
Energy Cost for Active Materials ($/kWh)	146
Power Cost for Active Materials ($/kW)	520

6.3 **Battery Cost Comparison**

Shown in Table 6.6, the active materials energy cost for BatteryAlpha, the LiBr-KBr battery system, and the LiCl-KCl off-eutectic battery system are within (~4$/kWh) of one another. As expected, the electrolyte energy cost for both of the multi-cation electrolyte systems was found to be lower than that for BatteryAlpha; although, in the case of the LiCl-KCl off-eutectic system not significantly so only (~2$/kWh) less expensive. The anode energy cost for both of the multi-cation electrolyte systems was found to be (~9$/kWh) more costly than the anode energy cost for BatteryAlpha. This is expected because BatteryAlpha has a pure lithium anode that utilizes all of its lithium for battery capacity whereas use of the Li-Mg alloy anode in the multi-cation electrolyte systems forces some lithium to remain unused in the anode. The power cost for BatteryAlpha was found to be (~ 100 $/kW) less expensive than the LiBr-KBr system and (~200 $/kW) less expensive than the LiCl-KCl. This is expected because the values in Table 6.6 were derived using observed efficiencies for BatteryAlpha, the LiBr-KBr system, and the LiCl-KCl system at current densities of 0.275 A/cm^2, 0.225 A/cm^2, and 0.175A/cm^2 respectively.

Table 6.6: Cost Comparison of Battery Systems

	BatteryAlpha	**Li-Mg/LiBr-KBr/Sb-Pb**	**Li-Mg/LiCl-KCl/Sb-Pb**
Energy Cost for Cathode ($/kWh)	68	68	66
Energy cost for Anode ($/kWh)	27	36	35
Energy Cost of ELC ($/kWh)	47	38	45
Energy Cost for Active Materials ($/kWh)	142	142	146
Power Cost for Active Materials ($/kW)	292	386	520

Chapter 7 – Conclusions

In this work lithium-magnesium was proven to be a viable anode in a high temperature Li-Mg/LiCl-LiF-LiI/Sb-Pb battery. Performance metrics for the Li-Mg battery system, shown in Table 7.1, were found to be comparable to the Li/LiCl-LiF-LiI/Sb-Pb system.[4] In addition, the Li-Mg system offered a low voltage penalty when compared to its pure lithium counterpart system, estimated to be (~0.03V) in the charge state and (~0.07V) in the discharge state.

Table 7.1: Performance Summary for Different Chemistries

	Li-Mg/LiCl-LiF-LiI/Sb-Pb	**Li-Mg/LiBr-KBr/Sb-Pb**	**Li-Mg/LiCl-KCl/Sb-Pb**
Cycles Demonstrated	120	70	75
Temperature (^{0}C) $^{\alpha}$	450	440	490
Current Density (A/ cm^2)$^{\alpha}$	0.275	0.225	0.175
Energy Efficiency (%)	63	62	67
Columbic Efficiency (%)	97	98	97
Charge Capacity Utilization (%)	96	93	90
Discharge Capacity Utilization (%)	93	91	89
Resistance (Ohm)	0.1 $^{\beta}$	0.05	0.05
Leakage Current (Amp)	0.009	0.008	0.005
Energy Cost for Active Materials ($/kWh)*	-	142	146
Power Cost for Active Materials ($/kW)*	-	386	520

$^{\alpha}$ The performance metrics for each battery system was observed at the temperature and current conditions specified in the table. $^{\beta}$ This resistance value is higher than expected due to use of screw clamps instead of set screws for the lead connection. (Outlined further in section 1.3)

The alloy anode approach to limiting the reactivity and solubility of lithium in the presence of multi-cation electrolytes proved to be effective. The LiBr-KBr and LiCl-KCl off-eutectic multi-cation electrolyte systems explored in this study were observed to cycle over 70

cycles and achieve impressive performance metrics outlined in Table 7.1. SEM and EDS confirmed stability of the each mutli-cation electrolyte with its anode and cathode.

The Li-Mg/LiBr-KBr/Sb-Pb and Li-Mg/LiCl-KCl/Sb-Pb multi-cation electrolyte systems were limited to temperatures ($\geq 440^0$C) and ($\geq 490^0$C) respectively for successful operation at the current densities listed in Table 7.1. For the Li-Mg/LiCl-KCl/Sb-Pb system the poor performance at temperatures (≤440°C: close to the electrolyte's melting point value) is correlated to salt solidification caused by either displacement reaction, concentration polarization during cycling, or temperature variation at the interface from entropic heat. In addition, for the Li-Mg/LiBr-KBr/Sb-Pb system this can most likely be attributed to complications arising from Li-Mg solid phase at low temperatures (~410^0C).

In terms of cost, both the Li-Mg/LiBr-KBr/Sb-Pb and the Li-Mg/LiCl-KCl/Sb-Pb systems achieved an active materials cost of (<150$/kWh), which is less expensive than the targeted cost metric. (Table 7.1) In addition, these multi-cation electrolyte systems achieved active materials energy costs comparable to BatteryAlpha. (Section 6.3) A cost comparison with BatteryAlpha conveyed that electrolyte energy cost for the LiBr-KBr and LiCl-KCl systems were (~ 9$/kWh) and (~ 2$/kWh) less expensive respectively. Although, it is important to note that, using a Li-Mg anode was found to be (~9 $/kWh) more expensive than using a pure lithium anode. (Section 6.3) In addition, due to the fact that the LiBr-KBr and LiCl-KCl systems were limited to low current densities (< 0.275 A/cm^2) at temperatures ($\leq 490^0$C) the power energy cost for these systems in comparison to BatteryAlpha was more expensive by (~100 $/kW) and (~200$/kW) respectively.

Future work will involve demonstrating successful operation of multi-cation electrolyte battery systems that can operate at higher current densities (~0.275 A/cm^2) and temperatures

(<400^{0}C). This will involve redesigning the Li-Mg anode such that it has phase stability at temperatures (<400^{0}C) and working with other low cost multi-cation electrolytes that have robust phase stability with varying composition (e.g., LiCl-KCl eutectic). Theoretically, allowing these multi-cation electrolyte systems to operate at lower temperatures should further limit the lithium displacement reaction from occurring (Equation 1.3) as well as lithium solubility in the electrolyte such that the battery is even more stable. Thus, knowing that multi-cation salts can successfully function in LMBs, there is a large window of opportunity to explore lower cost and higher efficiency electrolyte systems.

Bibliography

[1] Bradwell, D., D. Sadoway, and G. Ceder, *Technical and economic feasibility of a high temperature self-assembling battery, in Materials Science and Engineering.* 2006, Massachusetts Institute of Technology: Cambridge.

[2] Bradwell, D., *Liquid Metal Batteries: Ambipolar Electrolysis and Alkaline Earth Electroalloying Cells.* 2010, Massachusetts Institute of Technology: Cambridge.

[3] Masset, P., and R.A. Guidotti, *Thermal activated (thermal) battery technology part II. molten salt electrolytes.* 2007, Journal of Power Sources, 164, 397–414.

[4] Janz, G. J., *Thermodynamic and Transport Properties of Molten Salts: Correlation Equations for Critically Evaluated Density, Surface Tension, Electrical Conductance, and Viscosity Data.* 1988, J. Phys. Chem. Ref. Data, 17, Suppl. 2.

[5] Kim, H., et al., *Liquid metal batteries: past, present, and future*. 2012, Chem. Rev., 10.1021/cr300205k.

[6] Vissers, D.R., L. Redey, and T.D. Kaun, *Molten salt electrolytes for high-temperature lithium cells.* 1989, Journal of Power Sources, 26, 37-48.

[7] Zhang, W., *A review of the electrochemical performance of alloy anodes for lithium-ion batteries.* 2011, Journal of Power Sources, 196, 13-24.

[8] Kevorkov D.G., Gröbner J., Schmid Fetzer R., Pavlyuk V.V., Dmytriv G.S., and Bodak O.I., *The ternary Gd-Li-Mg system: phase diagram study and computational evaluation*. 2001, J. Phase Equilib., Vol. 22, p 34-42.

[9] Thomas, B. R., *Free energy of formation of binary compounds.* 1971, MIT Press, Cambridge, MA.

[10] N.P., *Potassium chloride with best price*. Lianyungang Tongyuan Chemical Industry Co., Ltd. 10 Mar. 2013. Web. 13 Mar. 2013.

[11] N.P., *Lithium bromide*. Weifang Union Biochemistry Co., Ltd. 11 Mar. 2013. Web. 13 Mar. 2013.

[12] N.P., *Factory price potassium bromide industrial grade*. Taian Yonghe Chemical Co., Ltd. 7 Nov. 2012. Web. 13 Mar. 2013.

[13] N.P., *Industry grade lithium chloride*. Nanjing Stable Trading Co., Ltd. 8 Aug. 2012. Web. 13 Mar. 2013.

[14] N.P., *Potassium Iodide 99%*. Zhuhai Yazhongxing Biological Technology Co., Ltd. 6 Dec. 2012. Web. 13 Mar. 2013.

[15] N.P., *Potassium Iodide 99%*. Zhuhai Yazhongxing Biological Technology Co., Ltd. 6 Dec. 2012. Web. 13 Mar. 2013.

[16] N.P., *KBr-LiBr.* FactSage: FTsalt-FACT Salt Phase Diagrams. 13 Mar. 2012. Web. 13 Mar. 2013.

[17] N.P., *KCl-LiCl.* FactSage: FTsalt-FACT Salt Phase Diagrams. 13 Mar. 2012. Web. 13 Mar. 2013.

[18] Burke, P., *Couples cost.* GroupSadoway presentation, MIT. 30 Aug. 2012.

[19] N.P, *Lithium fluoride industry grade.* Nanjing Stable Trading Co., Ltd. 11 Jul. 2012. Web. 13 Mar. 2013.

[20] N.P., *Sodium chloride (refined salt/industrial salt).* Wuhan Xinxing Kwan On Imp. & Exp. Trade Co., Ltd. 16 May. 2012. Web. 13 Mar. 2013.

[21] N.P., *98% sodium fluoride.* F-Aluminum import and export trade (Yunnan) Co., Ltd. 6 Mar. 2013. Web. 13 Mar. 2013.